FISEVIER

Contents lists available at ScienceDirect

Global and Planetary Change

journal homepage: www.elsevier.com/locate/gloplacha



Iron oxide tracers of ice sheet extent and sediment provenance in the ANDRILL AND-1B drill core, Ross Sea, Antarctica



Stefanie Brachfeld ^{a,*}, Juliana Pinzon ^{a,b}, Jason Darley ^a, Leonardo Sagnotti ^c, Gerhard Kuhn ^d, Fabio Florindo ^c, Gary Wilson ^e, Christian Ohneiser ^f, Donata Monien ^{d,g}, Leah Joseph ^h

- ^a Department of Earth and Environmental Studies, Montclair State University, Montclair, NJ 07043, USA
- ^b Department of Biology and Molecular Biology, Montclair State University, Montclair, NJ 07043, USA
- ^c Istituto Nazionale di Geofisica e Vulcanologia, Via di Vigna Murata 605, I-00143 Rome, Italy
- ^d Alfred-Wegener-Institut Helmholtz-Zentrum für Polar- und Meeresforschung, Am Alten Hafen 26, D-27568 Bremerhaven, Germany
- ^e Department of Marine Science, University of Otago, PO Box 56, Dunedin, New Zealand
- f Department of Geology, University of Otago, PO Box 56, Dunedin, New Zealand
- ^g Institute for Chemistry and Biology of the Marine Environment, Carl-von-Ossietzky University of Oldenburg, PO Box 2503, 26111 Oldenburg, Germany
- ^h Department of Environmental Studies, Ursinus College, Collegeville, PA 19426, USA

ARTICLE INFO

Article history: Received 31 March 2013 Received in revised form 8 September 2013 Accepted 23 September 2013 Available online 2 October 2013

Keywords: ANDRILL Antarctic Ice Sheet rock magnetism sediment provenance electron microscopy

ABSTRACT

The AND-1B drill core recovered a 13.57 million year Miocene through Pleistocene record from beneath the McMurdo Ice Shelf in Antarctica (77.9°S, 167.1°E). Varying sedimentary facies in the 1285 m core indicate glacial-interglacial cyclicity with the proximity of ice at the site ranging from grounding of ice in 917 m of water to ice free marine conditions. Broader interpretation of climatic conditions of the wider Ross Sea Embayment is deduced from provenance studies. Here we present an analysis of the iron oxide assemblages in the AND-1B core and interpret their variability with respect to wider paleoclimatic conditions. The core is naturally divided into an upper and lower succession by an expanded 170 m thick volcanic interval between 590 and 760 m. Above 590 m the Plio-Pleistocene glacial cycles are diatom rich and below 760 m late Miocene glacial cycles are terrigenous. Electron microscopy and rock magnetic parameters confirm the subdivision with biogenic silica diluting the terrigenous input (fine pseudo-single domain and stable single domain titanomagnetite from the McMurdo Volcanic Group with a variety of textures and compositions) above 590 m. Below 760 m, the Miocene section consists of coarse-grained ilmenite and multidomain magnetite derived from Transantarctic Mountain lithologies. This may reflect ice flow patterns and the absence of McMurdo Volcanic Group volcanic centers or indicate that volcanic centers had not yet grown to a significant size. The combined rock magnetic and electron microscopy signatures of magnetic minerals serve as provenance tracers in both ice proximal and distal sedimentary units, aiding in the study of ice sheet extent and dynamics, and the identification of ice rafted debris sources and dispersal patterns in the Ross Sea sector of Antarctica.

© 2013 Elsevier B.V. All rights reserved.

1. Introduction

The Antarctic Drilling (ANDRILL) Program is a multinational collaborative effort between Germany, Italy, New Zealand, and the United States, which has thus far conducted two field seasons in the western Ross Sea (Naish et al., 2009; Fielding et al., 2011). ANDRILL is the most recent in a series of collaborative international drilling programs whose goals include recovery of ice proximal records in order to study the dynamics of the Antarctic Ice Sheet (AIS), its fringing ice shelves and outlet glaciers at tectonic to modern timescales, including the earliest formation and subsequent evolution of the AIS, its volume and areal

extent, causes and effects of ice sheet and shelf collapse, behavior of the AIS during past episodes of global warmth, and the feedbacks between the Antarctic cryosphere and the global climate system. This information will aid in predicting how the Antarctic cryosphere may respond to future climate change, particularly with regard to the rate and amplitude of sea level rise. Determining this information from distal sites alone is challenging where the Antarctic signal is convolved with local environmental and tectonic processes, and for which the AIS is manifested as a single entity rather than as discrete signals of West Antarctic Ice Sheet (WAIS), East Antarctic Ice Sheet (EAIS), and Antarctic Peninsula Ice Cap (APIC) evolution.

Our study focuses on results from the AND-1B succession, which was recovered during the austral summer of 2006–07 at the McMurdo Ice Shelf site at 77.9°S, 167.1°W (Fig. 1). The McMurdo Ice Shelf is a portion of the Ross Ice Shelf that occupies McMurdo Sound between Ross Island,

^{*} Corresponding author. Tel.: +1 973 655 5129. E-mail address: brachfelds@mail.montclair.edu (S. Brachfeld).

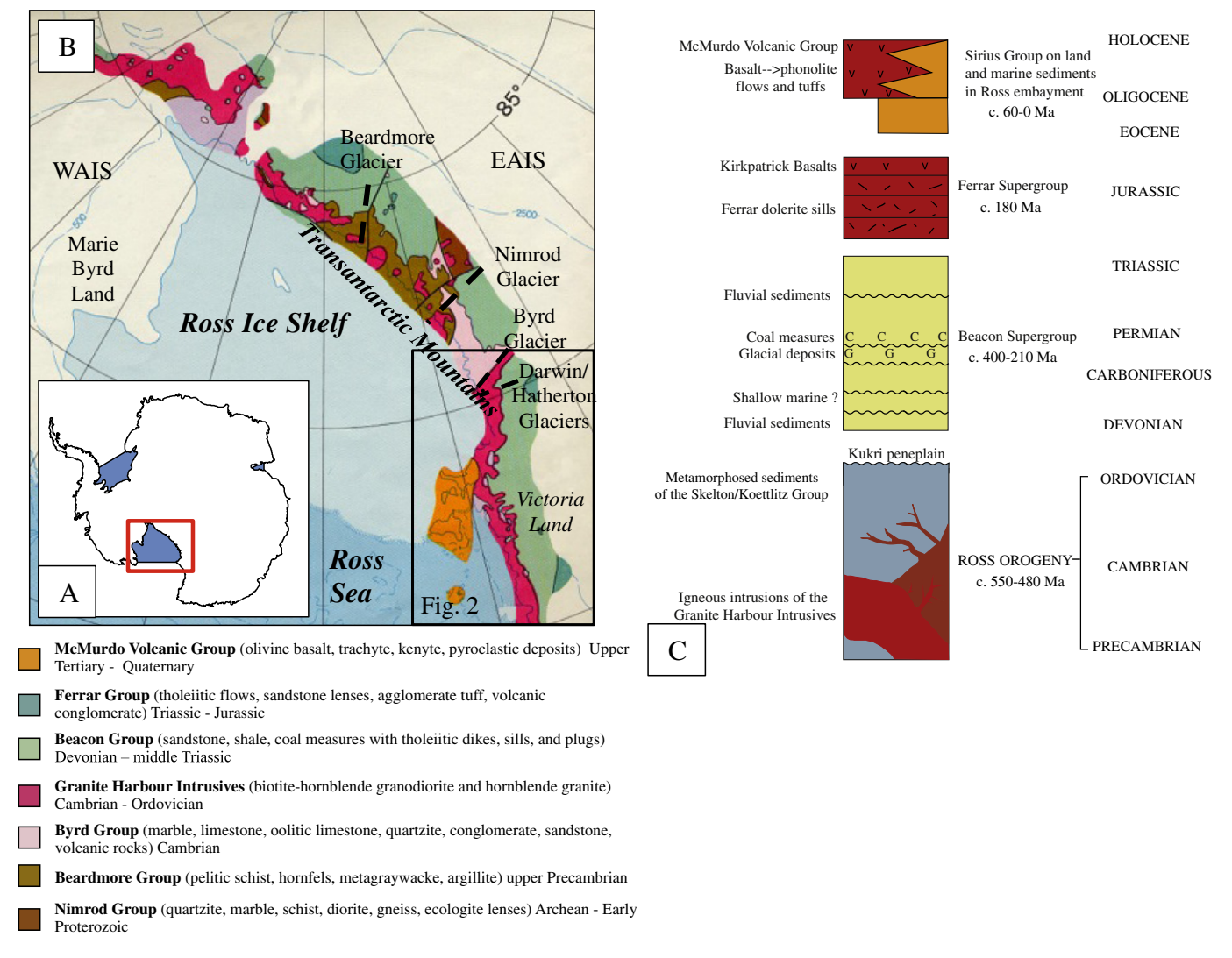


Fig. 1. A. (Inset) Location map showing the Ross Sea Embayment, Antarctica. (B) Geology of the western Ross Sea (after Licht et al., 2005). (C) Lithostratigraphic column summarizing the geologic history of the western Ross Sea.

White Island, and Black Island (Fig. 1). The AND-1B core comprises a 1285-m thick sedimentary section that was deposited in a flexural moat surrounding Ross Island, and has been dated back to 13.57 Ma (Wilson et al., 2012).

Here we examine the rock magnetic properties, iron oxide (hereafter Fe-oxide) textures and composition from the AND-1B drill core (with a focus on diamictites) and from the lithologic rock units that supply sediment to the western Ross Sea. Diamictites are deposited in sub-ice or ice-proximal environments and record the properties of the bedrock over which the ice flowed en route to the ice sheet terminus. Relative to mudstone and diatomite units in the AND-1B core, the diamictites should be free of the effects of sediment redistribution by ocean currents. We assess the Fe-oxide assemblages of diamictites to determine if they possess distinctive morphologies, compositions, and rock magnetic properties that can be used to trace sediment provenance, which would enable a means of identifying changes in ice sheet behavior such as a shift in the location or direction of ice flow through key Transantarctic Mountain (TAM) glaciers. To do this, we characterize the Fe-oxide assemblages and magnetic properties of the McMurdo Volcanic Group (MVG) and TAM lithologies to gain a better understanding of the starting mineral assemblage supplied to the Ross Sea, and compare these with Fe-oxide assemblage properties of the AND-1B diamictites.

2. Study area

The Ross Embayment sits at the boundary between East Antarctica and West Antarctica. The TAM form the western and southern boundaries of the embayment and Marie Byrd Land comprises the eastern boundary (Fig. 1). The embayment is occupied by the Ross Ice Shelf, which is fed by ice streams draining the WAIS and by outlet glaciers from the EAIS emerging from the TAM. A major goal of the ANDRILL Program is to evaluate the dynamics of the WAIS and EAIS through time. One method to monitor each ice sheet's past contribution to the Ross Ice Shelf is to trace the sediment that each ice sheet supplied to the Ross Embayment, a technique referred to as provenance tracing.

3. Provenance tracing and regional geology

The terrigenous material deposited at the AND-1B site is the product of glacial marine sedimentation processes, primarily the emplacement of diamict below grounded ice or immediately seaward of the grounding line, turbidity currents and release of debris-laden meltwater plumes seaward of the grounding line, basal melting in the sub-ice shelf cavity, and deposition of ice rafted debris (IRD) from calving and melting icebergs during open marine conditions. Clast lithology and

bulk geochemistry studies on the AND-1B core indicate two major source regions for the terrigenous sediment, the TAM and the MVG (Pompilio et al., 2007; Talarico and Sandroni, 2009; Monien et al., 2012; Talarico et al., 2012). The existence of these datasets provides a unique opportunity to test the utility of Fe-oxide and magnetic provenance tracers against the properties of the known source materials.

Fe-oxide provenance tracers have long been utilized in the Arctic Ocean (Darby and Bischof, 1996). The development of Fe-oxide provenance tracers for the western Ross Sea is based on the observed differences in the bedrock geology and magnetic petrography of the source regions. The geology of the regions bordering the Ross Sea is described in detail in Licht et al. (2005) and Talarico et al. (2012) and briefly summarized here (Fig. 2). The term "Basement" is used here to encompass late Precambrian to early Paleozoic metasediments of the Koettlitz Group, which are exposed in the TAM immediately west of the AND-1B site and contain gneiss, schist, quartzite, and marble within the

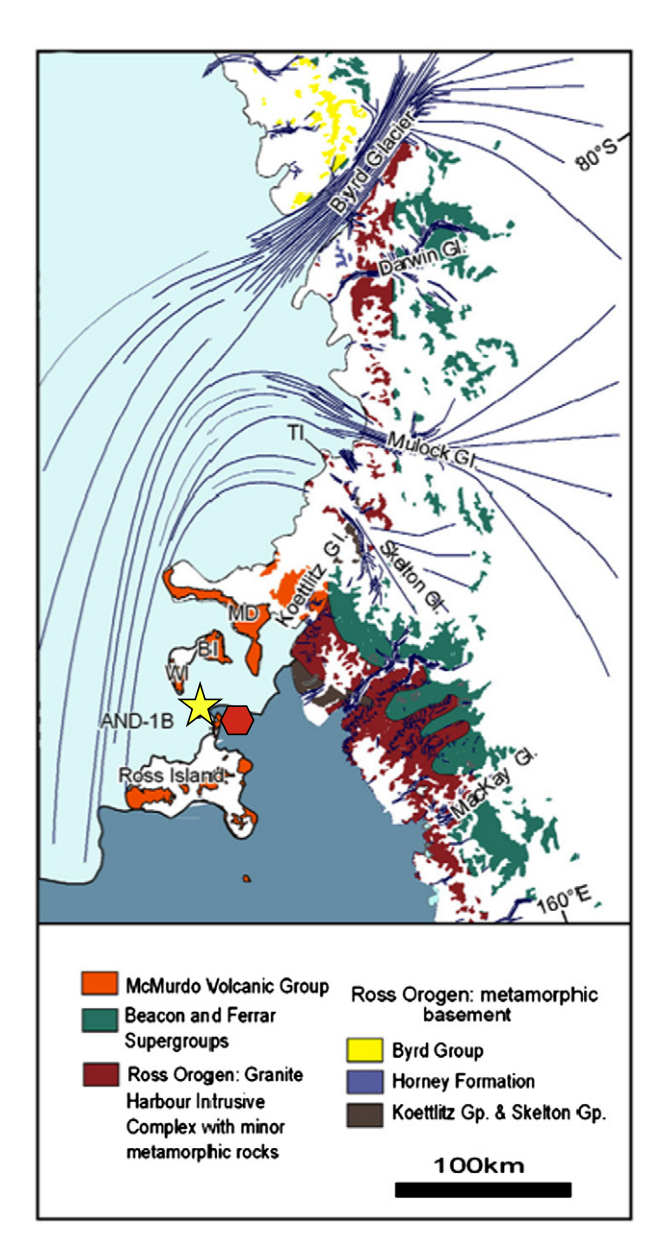


Fig. 2. The McMurdo Sound region showing the location of the AND-1B drill site (yellow star), Smith–McIntyre Grab NBP07-02 SMG1 (red hexagon), and outcrops of the units discussed in this study.

After Talarico et al. (2012).

Ross Group (Gunn and Warren, 1962; Findlay et al., 1984). The southern TAM contain low to high-grade metamorphics including gneiss, schist, quartzite, marble, and hornfels, occasionally intruded by diorite and lenses of ultramafic rock. The Basement rocks were intruded by the granitoids of the early Paleozoic Granite Harbor Intrusive Complex (GHIC), which was emplaced during the Ross Orogen (Gunn and Warren, 1962). These are overlain by the Devonian-Triassic clastic, glacial and fluvial sediments of the Beacon Supergroup (Barrett, 1991). This sequence was intruded by dolerite dikes and sills of the Ferrar Group during the initial break up of Gondwana (Heimann et al., 1994; Encarnación et al., 1996; Elliot and Fleming, 2000; Airoldi et al., 2012). Nearest to the AND-1B drill site are the MVG volcanic centers, consisting of basalts and trachytes emplaced within the last 24 Myr (Kyle, 1990a,b; Kyle et al., 1992; Di Roberto et al., 2010; Martin et al., 2010). We demonstrate here that there are measurable differences in the Fe-oxide textures and compositions and the magnetic signatures of the source regions that are transferred to the sediment deposited in the western Ross Sea.

4. Methods

Samples for rock magnetic analyses were collected every 1–4 m along the length of the AND-1B drill core. Samples for Fe-oxide microscopy and x-ray microanalysis were collected from diamictite units approximately every 100–150 m down core and are indicated by blue stars (thin sections) and red circles (grain mounts) in Figs. 3 and 4. A total of 94 bedrock samples from the TAM Basement, GHIC, Beacon Supergroup, Ferrar Group, and MVG were provided by the U.S. Polar Rock Repository located at the Byrd Polar Research Center, Ohio State University. These samples come from Northern Victoria Land (NVL), Southern Victoria Land (SVL), the Central Transantarctic Mountains (CTAM) and Southern Transantarctic Mountains (STAM), and are described in supplemental online Table S1. Samples were selected to capture a range of lithologies. A surface sediment grab from U.S. Antarctic Program cruise NBP07-02 augmented the MVG sample set in the McMurdo Sound area.

Low-field mass-normalized magnetic susceptibility (χ_{LF}) was measured on an AGICO KLY-4 Kappabridge using freeze-dried material. Low-field magnetic susceptibility measurements on bedrock samples were performed on the largest piece available, typically between 5 and 40 g. Ferromagnetic susceptibility (χ_F) for all samples was calculated by subtracting the high-field slope (χ_{HF}) of the magnetization (M) vs. applied field (H) curve measured on a vibrating sample magnetometer from γ_{LF} . Magnetic hysteresis measurements were made on a Princeton Measurements Corp. micro-Vibrating Sample Magnetometer model 3900-04 at Montclair State University, NJ. Hysteresis loops were measured in a peak field of 1 T and field increments of 5 mT. Raw data were processed by using χ_{HF} (calculated between 0.7 T and 1 T) to remove the paramagnetic contribution to the induced magnetization, and then normalized by mass. The hysteresis parameters saturation magnetization (M_S), saturation remanence (M_R) and coercivity (H_C) were determined from the paramagnetic-corrected data. The coercivity of remanence (H_{CR}) was determined through the DC-demagnetization of a saturation isothermal remanent magnetization imparted in a 1 T field. For weakly magnetic bedrock samples with noisy hysteresis loops we report M_R as the saturation remanence imparted at 1 T at the start of the H_{CR} measurement. The S-ratio was measured by imparting a 1 T isothermal remanent magnetization, followed by the application of a 300 mT backfield, and calculating S as $M_{R~(-300~mT)}\ /\ M_{R~(1~T)}.$ We occasionally obtained S-ratios slightly greater than one, likely due to asymmetry in the shape of rock chips measured on the VSM and/or measurement using a VSM system, which is unshielded and susceptible to the presence of induced components of magnetization in the presence of the ambient laboratory field.

Thermomagnetic curves were measured on an AGICO KLY-4 Kappabridge equipped with a CS furnace using approximately 200–500 mg of dry sediment or rock chips. Magnetic susceptibility

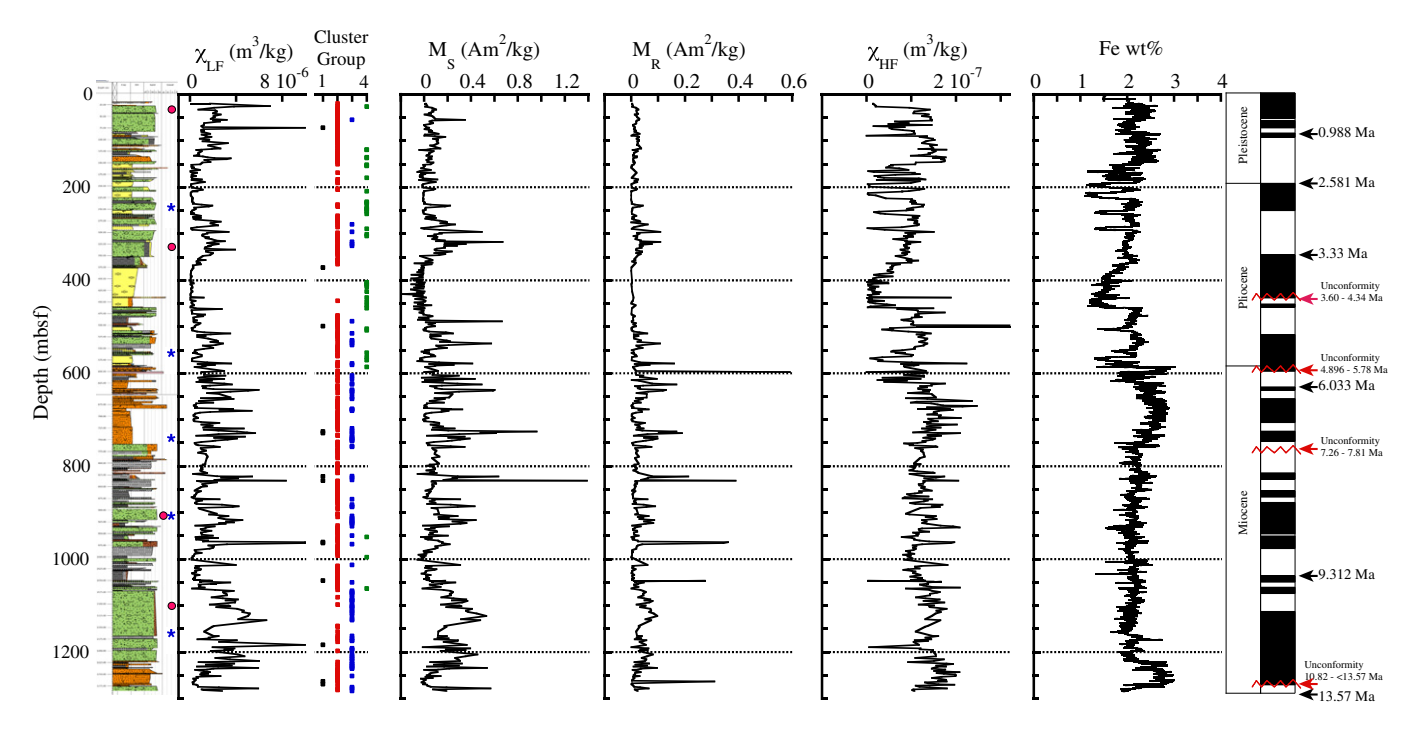


Fig. 3. AND-1B lithologic log from Krissek et al. (2007), concentration-dependent rock magnetic parameters, Fe abundance derived from x-ray fluorescence scanning (Monien et al., 2012), and core chronology (after Wilson et al., 2012). Lithologic units are coded as follows: Orange = volcanic and volcaniclastic units; green = diamictite; gray = mudstone, siltstone and sand-stone; yellow = diatomite. Rock magnetic parameters from left to right: low-field mass-normalized magnetic susceptibility ($\chi_{\rm IF}$), cluster group assignment, saturation magnetization ($M_{\rm S}$), saturation remanence ($M_{\rm R}$), high-field mass-normalized magnetic susceptibility ($\chi_{\rm HF}$), and wt.% Fe. Red circles indicate 45–500 µm grain mount horizons. Blue stars indicate thin section horizons. Cluster analysis performed with $\chi_{\rm LF}$, $\chi_{\rm HF}$, $M_{\rm S}$, $H_{\rm CR}$, and S ratios resulted in the identification of 4 unique clusters. Cluster groups 2 and 3 encompass diamictites in the upper and lower sections of the core, respectively. Cluster 4 corresponds with diatomites.

was measured during heating and cooling from 20 to 700 °C in a flowing argon gas atmosphere. Raw data were corrected for the furnace contribution and normalized by mass.

Thin sections and grain mounts were prepared to observe in-situ Feoxide mineral assemblages via electron microscopy. In many cases the most abundant Fe-oxides were micron to submicron grains within lithic

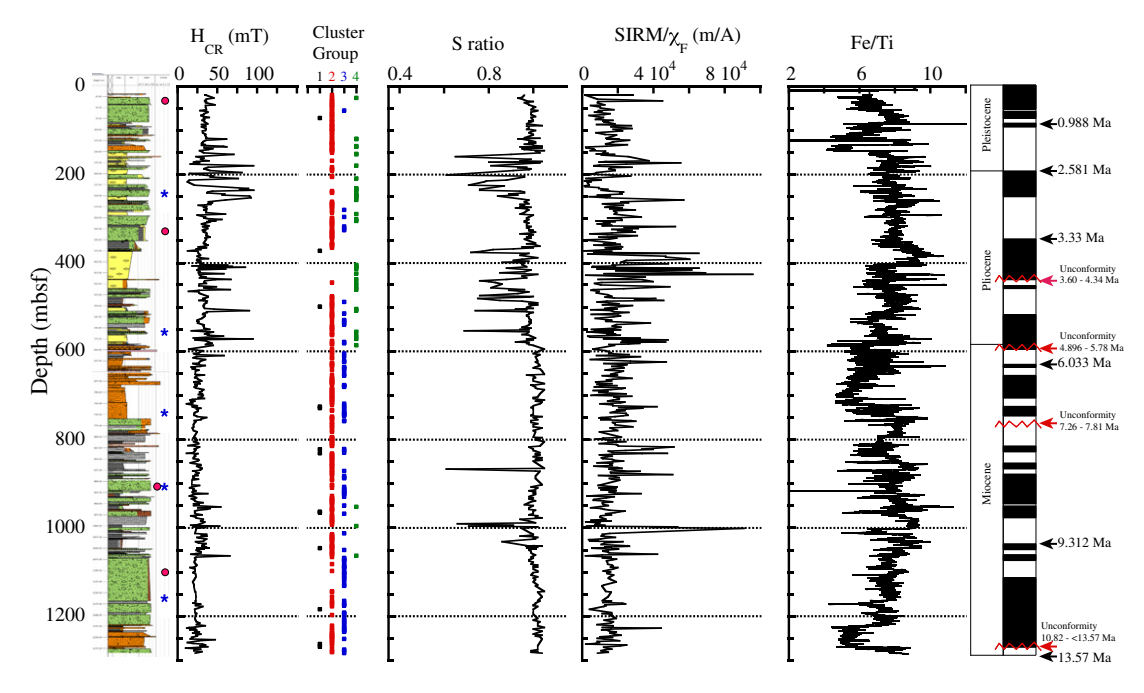


Fig. 4. AND-1B lithologic log from Krissek et al. (2007), grain size and mineralogy-dependent rock magnetic parameters, Fe/Ti ratio derived from x-ray fluorescence scanning (Monien et al., 2012), and core chronology (after Wilson et al., 2012). From left to right: coercivity of remanence (H_{CR}), cluster group assignment, S-ratio, saturation isothermal remanence magnetization normalized by ferromagnetic susceptibility (SIRM/ χ_F), and Fe/Ti ratio. χ_F (not shown) is calculated as $\chi_{LF} - \chi_{HF}$. Red circles indicate 45–500 μm grain mount horizons. Blue stars indicate thin section horizons.

clasts and were often smaller than the beam–specimen interaction volume (approximately 3–4 μm at 15 kV), precluding the ability to obtain a clean spectrum for quantitative analysis. Therefore, grain mounts were also prepared using the 45–500 μm size fraction (following Darby and Bischof, 1996) in order to examine larger Fe-oxides.

The 45-500 µm size fraction was wet sieved and then processed using a Franz magnetic separator. The magnetic fraction was examined under an Olympus SZ12 stereomicroscope. Grains with metallic luster were manually picked from the magnetic fraction, mounted in epoxy, polished, and carbon-coated. Polished specimens were examined using a Hitachi S-3400N Scanning Electron Microscope (SEM) equipped with a Bruker X-flash X-ray microanalysis system. Standardless quantitative analysis was performed using the Phi-Rho-Z standardless quantitative analysis routine in Bruker's Esprit 1.9.3 software. Tests of the Phi-Rho-Z routine on microprobe quality mineral standards yielded results within 0.05 to 1% relative of the published compositions for major elements (wt.% > 5%) and within 0.05-0.5% relative for minor elements (<5 wt.%). Raw wt.% was converted to wt.% oxides, with iron treated as Fe₃O₄. Values are reported in supplemental online Tables S2 (bedrock samples) and S3 (sediment samples). The number of cations per oxide formula unit was calculated on both 3-oxygen and 4-oxygen bases. Mineral assignments to either the titanomagnetite series or the titanohematite series were based on a combination of criteria including identification of textures associated with magnetite or hematite, where possible, (Ramdohr, 1969; Haggerty, 1991), determining which method yielded cation totals nearest to the target value of 2 or 3, respectively, for the 3-oxygen or 4-oxygen basis, hysteresis loop shape suggesting the presence of low or high coercivity minerals in a sample, and Curie temperature results.

The abundance of some elements between Al and Ba was measured using an AVAATECH X-ray fluorescence Core Scanner (XRF-CS) (Jansen et al., 1998). Peak intensities in total counts for Ti and Fe were converted to wt.% using calibration lines derived from discrete samples analyzed using inductively-coupled plasma optical emission spectrometry (Pompilio et al., 2007; Monien et al., 2012). Two-step log-likelihood cluster analysis was performed on rock magnetic parameters using IBM SPSS® version 20.

5. Lithostratigraphy

The AND-1B lithostratigraphy and chronology have been described in detail in Krissek et al. (2007), McKay et al. (2009), Naish et al. (2009), and Wilson et al. (2012). A brief discussion is given here. The upper 590 m of section consists of alternating diamictite and diatomite, often separated by thin mudstone beds (Fig. 3). The progression from diamictite to mudstone to diatomite represents the transition from a grounded ice sheet to floating ice shelf to an open marine environment at the AND-1B core site (McKay et al., 2009). Meter to decimeter thick diatomites are common in the upper section of the core. They are often thinly laminated with occasional dropstones (Konfirst et al., 2011).

The interval 590–760 m is dominated by volcanics and volcaniclastic sediment emplaced between 6 and 8 Ma (Wilson et al., 2012). Below 760 m the core is dominated by diamictites and mudstones. Where massive, the diamictites represent subglacial deposition and grounding of the Ross Ice Shelf on the seafloor (Krissek et al., 2007). Where stratified, the diamictites may indicate a fluctuating grounding line at the core site. Diatomites are absent and mudstones are thicker and more common in the lower section (Krissek et al., 2007).

6. Chronology

The integrated core chronology is described in Wilson et al. (2012) and summarized in Fig. 3. The chronology is based on a combination of tools including correlation of geomagnetic reversals with the geomagnetic polarity timescale (Wilson et al., 2012), recognition of diatom datums (Winter et al., 2012), and ⁴⁰Ar/³⁹Ar dating of volcaniclastic

material (Ross et al., 2012). The core contains numerous unconformities interpreted as glacial surfaces of erosion (GSE) formed during ice advances or sea level low-stands (McKay et al., 2009), and disconformities due to volcanism (Pompilio et al., 2007). The integrated chronostratigraphic data have been interpreted to define the Pleistocene interval from 0 to 191.75 m, and the Pliocene interval from 191.75 to 583.64 m (Wilson et al., 2012). The Miocene interval occurs below 583.64 m. The base of the AND-1B record is $^{40}{\rm Ar}/^{39}{\rm Ar}$ dated at 13.57 \pm 0.13 Ma (Ross et al., 2012) using volcaniclastic samples six meters above the base of the core.

7. Results

7.1. Rock-magnetic properties of AND-1B sediment

Diamictites and volcaniclastic units are characterized by high values of χ_{LF} , χ_{HF} , and M_S , while mudstones have intermediate values and diatomites have weak or negative values of χ_{LF} , χ_{HF} , and M_S , reflecting the high biogenic silica content in those units (Fig. 3, Table S4). The interval 0–590 m has lower amplitude and less variable values of χ_{LF} , χ_{HF} , and M_S . The interval 590–1285 m has higher amplitude and more variable concentration-dependent parameters (Fig. 3, Table S4). The parameter χ_{HF} , which tracks paramagnetic and diamagnetic mineral concentration, is positively correlated with wt.% Fe derived from XRF measurements (Fig. 3; Pompilio et al., 2007; Monien et al., 2012) with a Pearson correlation coefficient of 0.63.

Domain-state (grain size) dependent parameters are also correlated with lithology (Fig. 4). Diamictites, volcaniclastic units, and mudstones display pseudo-single domain hysteresis loops, which corresponds to the 1–10 μm size range for titanomagnetites (Day et al., 1977; Dunlop, 2002a,b). Diatomites are very weakly magnetic and yield diamagnetic M–H curves. Low applied field measurements such as H_C and M_R were noisy and occasionally indeterminate within diatomite samples. Domain state dependent parameters shift below 760 m, with M_R/M_S and H_{CR} suggesting coarsening of the magnetic mineral assemblage (Fig. 4, Table S4).

Mineralogy dependent parameters indicate the presence of low coercivity minerals such as magnetite, titanomagnetite, or magnetic iron sulfides throughout the core (Fig. 4). S-ratios are close to 1 in diamictites, mudstones, and volcaniclastic units. Diatomite units often yielded S-ratio values significantly greater than 1 and below 0.5, which were removed from the dataset for negative susceptibility intervals or intervals where the H_{CR} DC demagnetization curves were noisy. In general, diatomites displayed the lowest observed S-ratios (values less than 0.9) and also displayed the highest values of H_{CR} (values exceeding 50 mT). These observations suggest that diatomites either contain a greater amount of high-coercivity minerals than diamictite and mudstone lithologies, or that the expression of high coercivity minerals is only seen when the background sediment is weakly magnetic. SIRM/ χ_F values are generally below 30 kA/m in the diamictites in the upper half of the core, and below 20 kA/m between 590 and 1285 m (Fig. 4). Isolated spikes exceeding 40 kA/m are most common in the diatomites.

Thermomagnetic curves from diamictites in the upper section of the core show decreases in the heating curves at approximately 100–200 °C, 400–550 °C and 560–590 °C (Fig. 5). The 100–200 °C feature can be explained by either titanium-rich titanomagnetite or ilmenite (Dunlop and Özdemir, 1997). The loss of susceptibility between 470 and 550 °C can be explained by titanomagnetite with a moderate Ti content or titanomagnemite with a higher Ti content but elevated Curie temperature due to oxidation (Readman and O'Reilly, 1972). The loss of susceptibility between 560 and 590 °C is likely due to Ti-poor titanomagnetite and magnetite.

The 100–200 °C feature is absent in diamictites below 760 m. In the lower section of the core we observe an increase in χ_{LF} between room temperature and approximately 260 °C, followed by a peak in χ_{LF} between 260 and 280 °C (Fig. 5). A prominent drop in χ_{LF} is observed

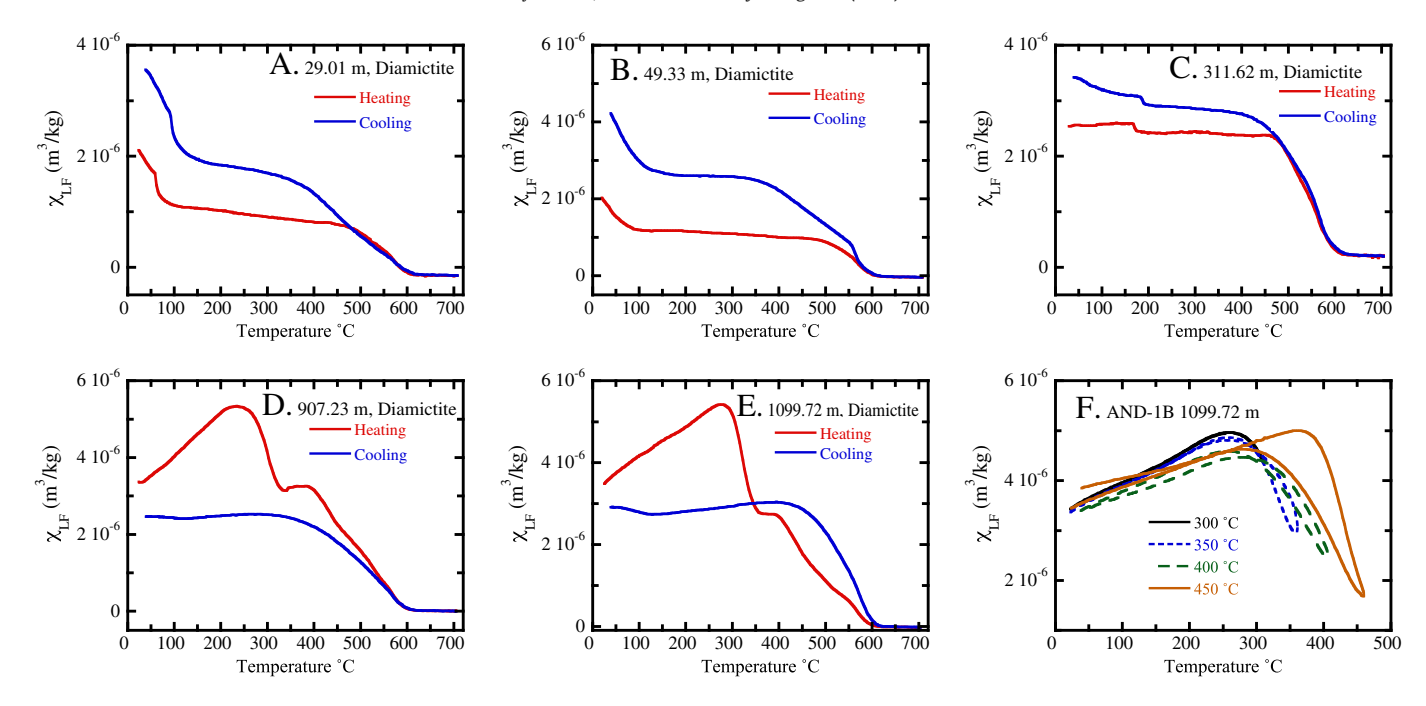


Fig. 5. Thermomagnetic curves for diamictite samples from the AND-1B core at (A) 29.01 m, (B) 49.33 m, (C) 311.62 m, (D) 907.23 m, and (E) 1099.72 m. Diamictites from the upper 590 m of the AND-1B core display a low-temperature order–disorder transition between 100 and 200 °C and a decrease in χ_{LF} that begins at 440–500 °C and continues to 600 °C. These features are also present in the cooling curves, but the heating and cooling curves are not perfectly reversible. These features are likely ilmenite, itianomagnetite or titanomagnetite or titanomagnetite, samples from the lower half of the core lack the 100–200 °C feature and instead show a rise in signal between 20 and 260 °C, followed by a loss of signal between 300 and 360 °C. The cooling curve is lower than the heating curve from 350 to 20 °C. Temperature cycling experiments (F) show reversible heating and cooling curves up to a peak heating temperature of 350 °C. These features are interpreted as unblocking of fine SSD grains below 260 °C and the inversion of maghemite to hematite between 300 and 360 °C.

between 300 and 360 °C, followed by a steady decrease in the intensity of χ_{LF} from 400 to 600 °C. The cooling curve is higher than the heating for the interval 700–350 °C, but lower than the heating curve from 350 to 20 °C. Repeated cycling at stepwise increasing temperature of a sample from 1099.72 m shows reversible thermomagnetic curves up to 350 °C (Fig. 5F). These observations are consistent with the presence of maghemite.

7.2. Magnetic petrography of AND-1B sediment

Diamictites from the upper 590 m of the AND-1B core contain Feoxide grains that are submicron up to $200\,\mu m$ in diameter. Fe-oxides smaller than 5–10 μm are abundant as inclusions within lithic fragments (Figs. 6, 7). Sub-micron grains outline plagioclase laths within volcanic lithics (Fig. 6B) and occur as euhedral grains within volcanic glass (Fig. 7A, D).

In the upper 590 m we observed homogeneous titanomagnetite grains with 1.7–1.9 Fe cations per formula unit (Table S3, Fig. 6G, H), substantial amounts of Mg, Al, and Ti, variable amounts of Cr, and minor amounts of Mn. Grains with oxidation exsolution textures are also common (Fig. 6D-F). We observed titanomagnetite host grains with 3 swarms of very-closely-spaced micron-sized ilmenite lamellae oriented in the {111} planes (Fig. 6D). Bulk compositions of these grains yield 2.3 to 2.8 Fe cations per formula unit on a 4-oxygen basis (Table S3). We observed Fe-rich host grains with two generations of exsolution, an earlier generation with 3 swarms of ilmenite lamellae and a later generation of hercynite lamellae, which cut the ilmenite bodies (Fig. 6E). The x-ray microanalysis data for many homogeneous and exsolved grains gave slightly better solutions for a 3-oxgyen basis even though the textures and cation substitution patterns are more consistent with spinels. Therefore, we speculate that the original titanomagnetite host grains have been oxidized to titanomaghemite.

Fe-oxides hosting lamellae are present in diamictites between 760 and 1285 m, but these grains are smaller than those observed between 0 and 590 m (Fig. 7). In addition, the lamellae tend to be coarser and have a wider spacing than those observed in the upper 590 m. In the interval 900–1285 m we observe more grains with homogeneous textures (Fig. 8). Fe-oxide grain mounts at 911.28 m and 1097.53 m show emulsion textures (small dark speckles) and homogeneous grains with smooth, oval-shaped pits formed by plucking of adjacent apatite and zircon grains (Figs. 8E, 9). We also observed Cr–Al–Mg-bearing titanomagnetite grains with 1.1–1.2 and 2.3–2.9 Fe cations per formula unit whose compositions match those observed in MVG bedrock and surface grab samples. Coarse grained, homogeneous, magnetite grains with little to no cation–substitution are common in the lower section, as are homogeneous ilmenite grains with up to 5% Mn (Table S3, Figs. 7, 8).

7.3. Rock-magnetic properties of MVG and TAM bedrock

Concentration dependent magnetic parameters χ_{LF} and M_S vary over nearly five orders of magnitude from 10^{-9} to 10^{-5} m³/kg and 10^{-4} to 10^{0} Am²/kg, respectively, for Ross Sea bedrock lithologies (Fig. 10A). MVG and Ferrar Group basalts, lavas, and dolerite have the highest χ_{LF} and M_S values, although the Ferrar Group has a two order of magnitude range of values for both parameters. Basement lithologies and Beacon Supergroup samples have uniformly weak χ_{LF} and M_S values (Fig. 10A). GHIC samples form two groups on a χ_{LF} vs. M_S plot. However, there is no clear explanation for these groups, which are independent of spatial location and rock type, and likely reflect heterogeneity among the rock chips measured on the VSM.

Hysteresis parameters behave as expected, with fine-grained mafic lithologies displaying higher values of M_R/M_S . The parameters M_R and H_C were often noisy or indeterminate in weakly magnetic Basement lithologies and Beacon Supergroup samples. Therefore, in calculating M_R/M_S we use the M_R value obtained at the beginning of the H_{CR}

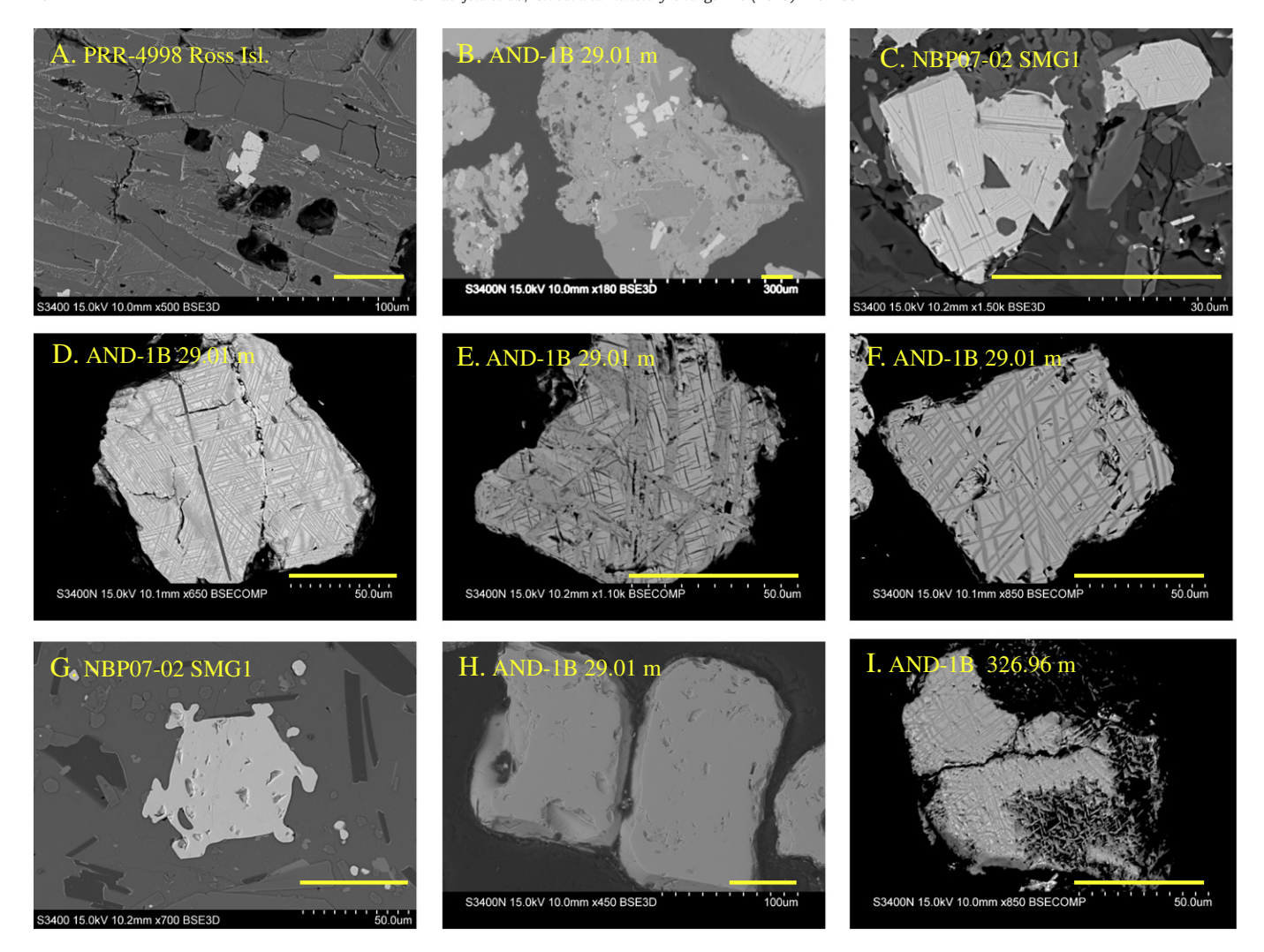


Fig. 6. Backscatter electron microscopy images from MVG bedrock samples and diamictites from the upper 590 m of the AND-1B core. The yellow scale bar in all images is 50 μ m long. (A) Polar Rock Repository (PRR) sample 4998 from Ross Island showing homogeneous euhedral titanomaghemite with composition Fe_{2.18}Ti_{0.66}Z_{0.15}O₄, where Z is the sum of Mg, Al, Cr, and Mn cations, and submicron magnetite outlining plagioclase laths. (B) A lithic clast from 29.01 m within the AND-1B drill core showing submicron oxides outlining plagioclase similar to those in panel A and titanomagnetite hosting multiple swarms of ilmenite lamellae (top center of image), which resemble the grains in panel C. (C) A light-gray fine-grained volcanic sample from NBP07-02 SMG1 containing titanomagnetite grains hosting multiple swarms of ilmenite lamellae. (D) Exsolved grain from AND-1B 29.01 m with three closely spaced swarms of thin ilmenite lamellae oriented in the {111} planes of titanomagnetite. (E) Fe-oxide grain with two generations of exsolution lamellae, one consisting of ilmenite (larger, lighter gray features) and a second consisting of smaller, darker, hercynite lamellae. (F) Spindle-shaped Ti-rich lamellae in a titanomaghemite host. (G) Homogeneous titanomaghemite with composition Fe_{1.85}Ti_{0.56}Mg_{0.32}Al_{0.20}Mn_{0.02}O₄ in a black crystalline basalt from NBP07-02 SMG1. (H) Homogeneous titanomaghemite grains from 29.01 m in the AND-1B core with composition Fe_{1.81}Ti_{0.056}Mg_{0.30}Al_{0.24}O₄, resembling those in panel G. (I) Exsolved titanomagnetite grain from 326.96 m in which the Fe-rich interlamellae regions have undergone dissolution.

measurement routine, for which we can compensate for low signal strength with a longer measurement averaging time. We display these parameters on a modified Day Plot with H_{CR} on the horizontal axis (Fig. 10C, D). Basement lithologies and GHIC samples display typical multidomain (MD) loops and have S ratios near to 1 (Fig. 10E). Ferrar Group samples plot slightly higher and to the left on the modified Day Plot, indicative of finer pseudo-single domain grains. Ferrar Group samples also have S ratios near to 1 (Fig. 10C). MVG samples have PSD to SSD hysteresis parameters and S ratios near to 1, though reddish-brown basalt lithics from the NBP07-02 surface sediment grab have S-ratios of 0.92–0.93. Beacon Supergroup samples and Basement gneisses and sandstones also have low S-ratios ranging from 0.8 to 0.9.

Thermomagnetic curves from MVG samples show a decrease in signal from 20 to 200 °C and 400–550 °C, suggestive of ilmenite and either titanohematite or titanomagnetite with intermediate Ti content (Fig. 11). The heating and cooling curves are not reversible, from which we infer the presence of titanomagnemite. Ferrar dolerite samples display a large drop in signal between 560 and 600 °C, with nearly

reversible heating and cooling curves. GHIC samples also display a large drop in signal between 560 and 600 °C, with cooling curves slightly higher than heating curves. Beacon Supergroup samples generally display a loss in signal between 550 and 600 °C, with varying degrees of alteration during heating. Basement metamorphics were very susceptible to alteration during heating, with a steady decay in signal from room temperature to 400 °C, followed by a large gain in signal between 400 and 550 °C as ferromagnetic minerals are formed during the measurement.

7.4. Magnetic petrography of MVG and TAM bedrock

The MVG bedrock samples consist of hand samples from Ross Island, Tent Island, Mount Morning, and gravel from a surface sediment grab collected in McMurdo Sound during NBP07-02 (see Tables S1 and S2). The gravel fraction of NBP07-02 SMG1 consists of glassy brown-colored vesicular basalt, black non-vesicular crystalline basalt, red vesicular basalt, and light gray fined-grained volcanics. Several populations

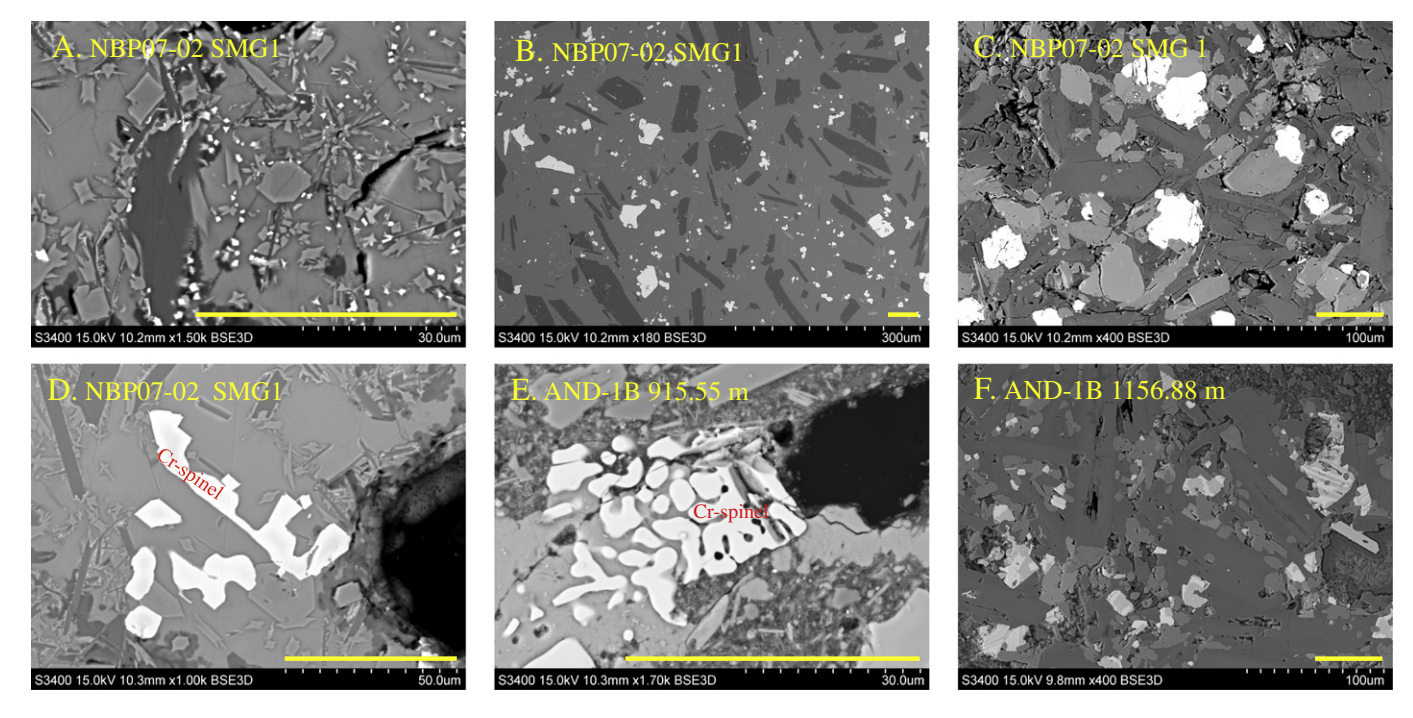


Fig. 7. Backscatter electron microscopy images from MVG bedrock samples and diamictites from the lower section of the core. The yellow scale bar in all images is 50 μm long. (A) Micron to submicron euhedral Ti-poor titanomagnetite in a glassy basalt from NBP07-02 SMG1. The small grain size precludes determination of a precise chemical composition. (B) Micron to coarse-grained titanomaghemite in a crystalline basalt sample from NBP07-02 SMG1. (C) Titanomagnetite with one to two swarms of ilmenite lamellae in a light-gray volcanic clast from NBP07-02 SMG1. Lamellae are both thicker and more widely spaced than the examples in Fig. 6. (D) Al-, Cr-, and Mg-rich spinels in a glassy basalt from NBP07-02 SMG1 with average composition Fe_{1.29}Al_{0.62}Cr_{0.46}Ti_{0.22}Mg_{0.42}O₄. (E) Al-, Cr-, and Mg-rich spinels in a diamictite sample at 915.55 m in the AND-1B core, with average composition Fe_{1.18}Al_{0.70}Cr_{0.41}Ti_{0.19}Mg_{0.49}O₄, resembling those in panel D. (F) Assemblage of titanomagnetite grains in a diamictite sample from 1156.88 m, with one or two swarms of broadly-spaced ilmenite lamellae, similar to those observed in panel C.

of Fe-oxides were observed in MVG samples. We observed two groups of homogenous titanomaghemite grains that are $10-50\,\mu m$ in diameter with 1.7-1.9 and 2.1-2.2 Fe cations per formula unit, and the remaining cations composed of Ti, Mg, Al, and Mn (Fig. 6). The second population consists of submicron Fe-oxides that outline laths of plagioclase feldspar (Fig. 6A). These are low-Ti titanomagnetites and are likely responsible for the thermomagnetic features between 560 and 590 °C in MVG samples. The third group consists of Cr-rich $20-30\,\mu m$ homogeneous Fe-Al-Cr-Mg-Ti oxides with average composition of Fe $_{1.29}$ Al $_{0.62}$ Cr $_{0.46}$ Ti $_{0.22}$ Mg $_{0.42}$ O4. The final group consists of $20-200\,\mu m$ titanomagnetite and titanomaghemite host grains containing 1-3 swarms of ilmenite lamellae. The host grains have 2.3-2.7 Fe cations per formula unit (Table S2).

Ferrar Group samples contain abundant Fe-oxides with homogenous textures that range in size from submicron up to 300 µm, though the majority are smaller than 50 µm (Fig. 8). We observed titanomagnetites with 2.7-3.0 Fe cations per formula unit and minor amounts of Ti, Al, and Mn. We also observed Mn-bearing ilmenite, and Cu-Fe sulfides in Ferrar Group samples. GHIC samples (Table S2, Fig. 9) contain coarse oxides up to 400 µm in diameter. The two main populations of oxides are homogenous ilmenite with 2-7 wt.% Mn and nearly pure magnetite with 2.9-3.0 Fe cations per formula unit. Several Ti-rich minerals are present in the Basement samples from the Koettlitz Glacier, Skelton Glacier, Darwin Glacier, and Byrd Glacier regions. These include ilmenite, titanite, and rutile. Ilmenites from these units contain not only several wt.% Mn, comparable to the GHIC samples, but also measurable Nb, the only bedrock group for which this trace element was above our x-ray system's detection limit. Gneisses from the Byrd Glacier region are also unique in that they contain 10-20 µm pyrite grains, often with magnetite rims and/or intergrowths along cracks (Table S2, Fig. 9).

8. Discussion

8.1. Productivity and diagenetic controls on rock-magnetic parameters

Rock magnetic properties of the AND-1B sediment sequence reflect the interplay of the properties of the source material, sediment transport process that modify the magnetic mineral assemblage (for example sorting based on grain size or mineral density), and processes specific to the depositional environment. To first order, the magnetic properties of the AND-1B sediment reflect the depositional environment and resulting lithologic unit. Diamictite and clastic units (sandstone and siltstone) exhibit higher χ_{LF} and M_S values than diatomites (Figs. 3–4). Diamictite and clastic units have χ_{LF} values comparable to those of the MVG and Ferrar Group samples (Fig. 10AB). Diatomites have χ_{LF} values that are 2-3 orders of magnitude weaker than the clastic units but still exceed the susceptibility of Basement, Beacon Supergroup, and GHIC lithologies (Table S1, Fig. 10AB). This requires the presence of strongly magnetic terrigenous material within the diatomites and is consistent with data that indicate that MVG-derived clasts dominate the clast assemblage within diatomites (Talarico et al., 2012).

A second order effect is a dichotomy between the magnetic mineral assemblage in diamictites in the upper 590 m and lower 525 m of the core. The diamictites between 0 and 590 m have lower values of χ_{LF} , M_S , M_R , and S-ratio, and higher values of H_{CR} and M_R/M_S . The reverse is true for diamictites between 760 and 1285 m (Fig. 10). These visual observations were confirmed using two-step cluster analysis based on the six input parameters χ_{LF} , χ_{HF} , M_S , M_R , H_{CR} , and S-ratio. The analysis resulted in the identification of four unique clusters (Figs. 3 and 4). Cluster 1 has only 13 members, which correspond to intervals with very high susceptibility, likely due to the presence of strongly magnetic lithic clasts. The majority of samples belong to cluster 2, which encompasses

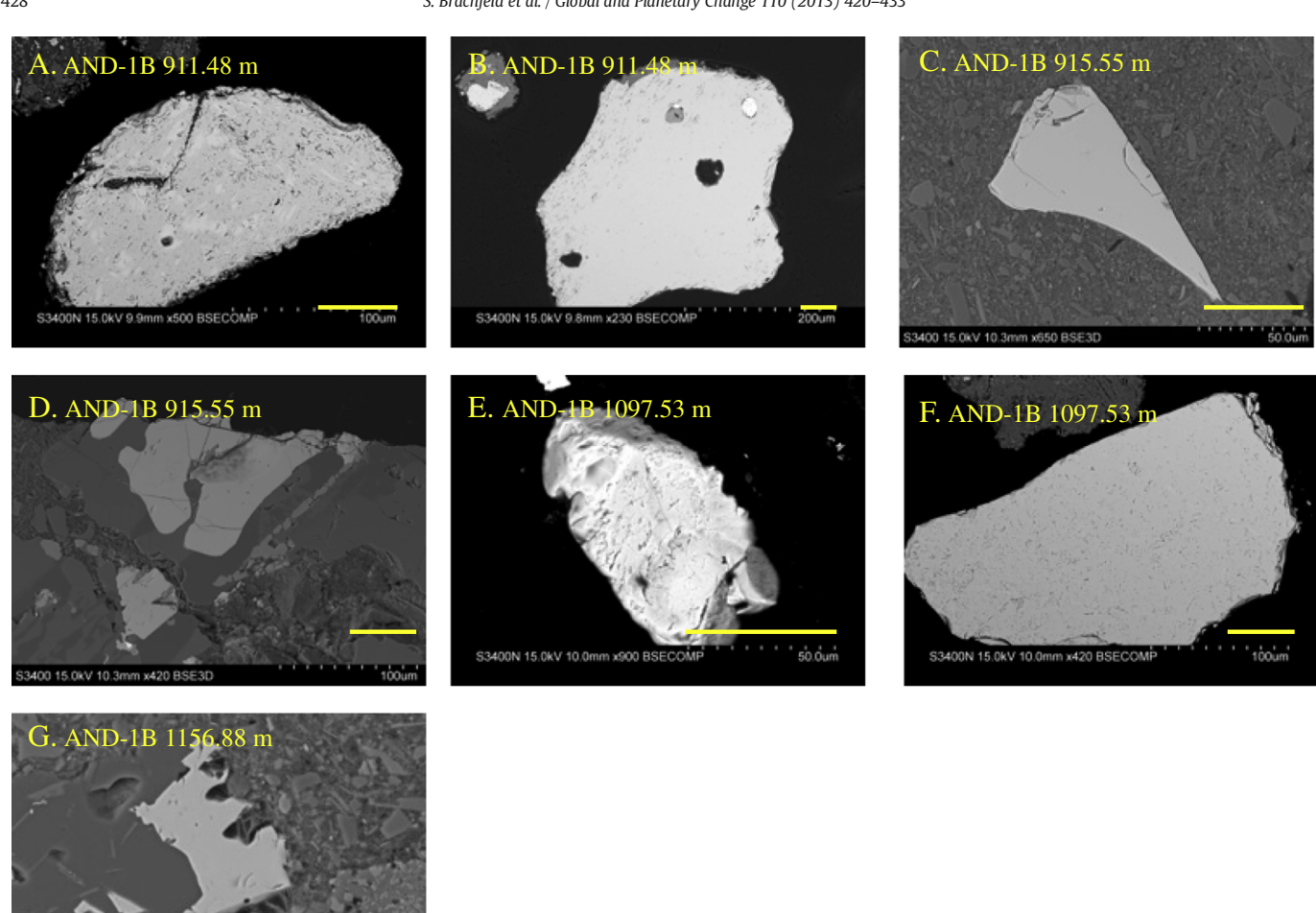


Fig. 8. Backscatter electron microscopy images from TAM bedrock samples and diamictites from the lower section of the core. The yellow scale bar in all images is $50\mu m$ long. (A) Magnetite grain from a diamictite unit at 911.48 m with small exsolution emulsions containing Al and Zn. Differential shading in the grain suggests patches of oxidation. (B) Mg-bearing ilmenite host grain (Fe_{0.78}Ti_{0.96}Mg_{0.24}Al_{0.02}O₃) from 911.48 m with a pyrite inclusion. (C) Magnetite grain in a diamictite unit from 915.55 m. (D) Homogeneous ilmenite grains from 915.55 m with average composition Fe_{0.98}Ti_{0.96}Mn_{0.04}Mg_{0.01}O₃. (E) Magnetite from a diamictite unit at 1097.53 m with oval pits from plucking of apatite and/or zircons grains. (F) Homogeneous ilmenite grain from 1097.53 m. (G) Homogeneous ilmenite grain from a diamictite unit at 1156.88 m with composition Fe_{0.93}Ti_{1.03}Mn_{0.04}O₃.

diamictites and clastic units along the entire length of the AND-1B drill core. Cluster 3 samples also include diamictites and clastic units, but cluster 3 members occur mainly below 460 m. Cluster 4 samples are from diatomite units.

The difference in concentration-dependent parameters between the upper and lower sections of the core is controlled in part by the amount of biogenic sediment present. The interval 0-590 m comprises the Pliocene and the early Pleistocene interval, which is marked by obliquitycontrolled alternations between diamictite and diatomite (McKay et al., 2009). Diatomites indicate retreat of the Ross Ice Shelf and potential collapse of the WAIS with extended periods of open water (Naish et al., 2009). Diamictites between 0 and 590 m contain diatoms and some intervals have biogenic silica content approaching 10% (McKay et al., 2009), suggesting that these units were emplaced near to the grounding line, in proximity to seasonally open water such that currents, turbidites, or reworking within the flexural moat could carry biogenic silica to the drill site at times when the drill site was seaward of the grounding line. The presence of biogenic silica dilutes the terrigenous sediment and reduces the amplitude of χ_{LF} in these units. Between 760 and 1285 m the diamictite units have no observable diatoms and no biogenic silica (McKay et al., 2009), therefore no dilution of χ_{LF} in this interval.

Dissolution of Fe-oxides in the upper 590 m of core may also contribute to the observed lower values of χ_{LF} and M_S with respect to the lower half of the core. We observed pyrite framboids throughout the core, indicating the occurrence of iron-sulfur diagenesis. Diagenetic alteration of the magnetic mineral assemblage should be greatest in the organic rich units (Berner, 1984). Diatomite thermomagnetic curves (not shown) were highly susceptible to alteration and growth of magnetite during heating, and we observe higher than average SIRM/ χ_F values within diatomites, suggesting the presence of ferrimagnetic iron sulfides (Peters and Thompson, 1998). Fine SSD and superparamagnetic (SP) Fe-oxides would be most susceptible to dissolution within the diatomites. SEM observation from a depth of approximately 327 m in the AND-1B core shows the dissolution of Fe-rich interlamellae regions between Ti-rich lamellae (Fig. 6I). However, coarsening of the residual magnetic mineral assemblage is not observed, likely because a large portion of SP and SSD Fe-oxides are protected within lithic clasts.

Enhancement of susceptibility in the lower section of the core may also be due to the presence of SP maghemite. The presence of maghemite is suggested by thermomagnetic curves from the diamictites below 760 m. The heating curves display an increase in χ_{LF} between 20 and 260 °C, followed by a drop in χ_{LF} between 300 and 360 °C. The cooling

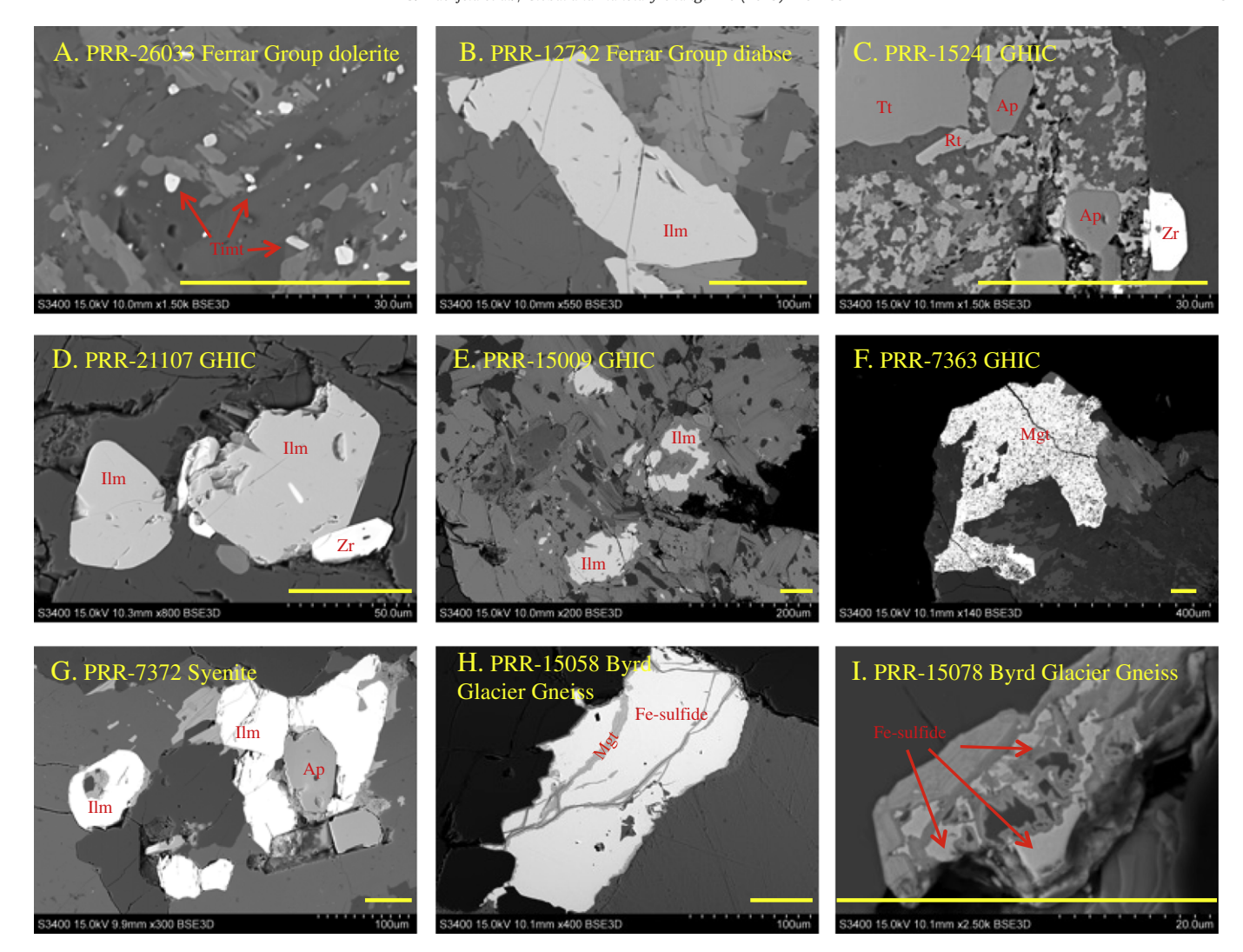


Fig. 9. Backscatter electron microscopy images from TAM bedrock samples and diamictites from the lower section of the core. The yellow scale bar in all images is $50 \,\mu m$ long. (A) $3-5 \,\mu m$ rounded grains of Ti-poor titanomagnetite from a Ferrar Group dolerite sill. These grains are close to the beam–specimen interaction volume. EDX spectra contained measurable Si, indicating contamination from the surrounding silicate minerals. However, the spectra suggest > 2.8-2.9 Fe cations per formula unit. (B) Ilmenite grain from a Ferrar Group diabase sample with composition Fe_{0.96}Ti_{0.98}Mg_{0.06}O₃. (C-F) GHIC samples, as follows: (C) a weakly magnetic grainte from the Skelton Glacier region containing ilmenite with average composition Fe_{0.84}Ti_{.05}Mg_{0.11}O₃. (E) A strongly magnetic GHIC sample containing ilmenite with average composition Fe_{0.84}Ti_{.05}Mg_{0.07}O₃. (F) A strongly magnetic GHIC sample containing extremely coarse-grained pure magnetite. (G-I) Basement lithologies as follows: (G) ilmenite and zircon-bearing syenite from the Skelton Glacier region. (H) Gneiss sample from the Byrd Glacier region containing Fe-sulfides.

curves are weaker than the heating curves (Fig. 11F, G). The Miocene diamictite thermomagnetic curves resemble those reported in loess-soil sequences in which the low temperature increase in χ_{LF} was attributed to the unblocking of SSD particles (Liu et al., 2005). The inversion of moderately strong maghemite to weakly magnetic hematite would explain the weaker χ_{LF} values in the cooling curves (Florindo et al., 1999; Liu et al., 2005). The most likely sources of maghemite for the AND-1B core are the sandstones and siltstones of the Beacon Supergroup, for which several samples were observed to have a reddish-brown color, χ_{LF} values above $1*10^{-7}\,\mathrm{m}^3/\mathrm{kg}$, and thermomagnetic curves suggestive of maghemite.

8.2. Construction of Fe-oxide provenance tracers for the Ross Sea

Each of the five major bedrock groups has distinctive signatures that are transferred to the sediment derived from these rocks. MVG bedrock samples have PSD to SSD hysteresis loops, some with wasp-waisting. The light gray and the crystalline black MVG volcanics contain the 100–200 °C feature in their thermomagnetic curves. This feature is present in the upper 590 m of the AND-1B

core where clast and geochemical data indicate a dominant MVG source, and absent below 760 m where the clast and geochemical data indicate a dominant TAM source (Monien et al., 2012; Talarico et al., 2012).

In matching thermomagnetic features to specific Fe-oxide populations we note that some of the compositions reported here, such as spinels with less than 2.4 Fe cations per formula unit, have theoretical Curie temperatures below 20 °C and should appear paramagnetic above room temperature (Dunlop and Özdemir, 1997). We propose that oxidation of both titanomagnetite host grains (to titanomagnemite) and ilmenite lamellae (to titanohematite) raises their order-disorder transition temperatures (Readman and O'Reilly, 1972). The 100–200 °C features could be due to either the homogeneous titanomaghemite grains or to oxidized ilmenite lamellae. The features between 400 and 550 °C are attributed to the titanomagnetite population with 2.4-2.7 Fe cations per formula unit. This interpretation also requires maghemitization to elevate the Curie temperatures. The submicron Fe-oxides encased in volcanic lithics and those that outline plagioclase laths are likely magnetite and responsible for the 560-590 °C Curie temperatures. The combination of PSD to SSD hysteresis loops, the 100-200 °C order-disorder

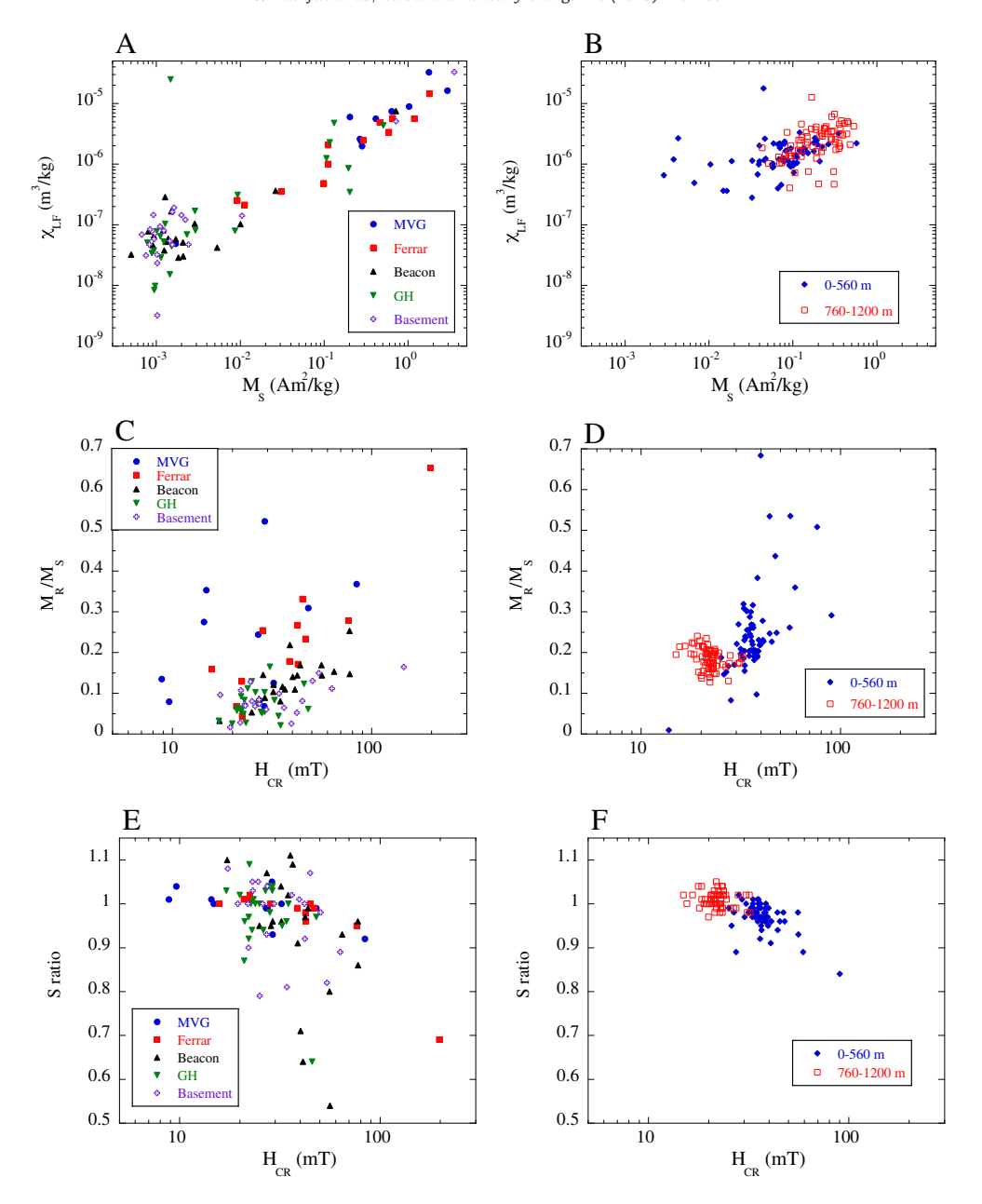


Fig. 10. (A) Bedrock sample χ_{LF} vs. M_S . (B) AND-1B diamictite χ_{LF} vs. M_S for samples from 0 to 590 m and 760–1285 m. (C) Bedrock sample M_R/M_S vs. H_{CR} on a modified Day Plot. (D) AND-1B diamictite samples M_R/M_S vs. H_{CR} on a modified Day Plot. In general, diamictite units from above 590 m have higher values of M_R/M_S and higher values of H_{CR} than their counterparts below 760 m, suggesting coarsening of the magnetic mineral assemblage in the lower portion of the core. (E) S-ratio vs. H_{CR} for bedrock samples. (F) S-ratio vs. H_{CR} for AND-1B diamictites.

transition, magnetite on plagioclase texture, high Mg, Al, and Cr contents, and $100-200\,\mu m$ grains with 1-3 swarms of ilmenite lamellae, all which commonly occur in the interval $0-590\,m$, are markers of the MVG.

Ferrar dolerite bedrock samples also have PSD to SSD hysteresis parameters, but without wasp-waisting. Ferrar Group samples have Curie temperatures very close to but slightly higher than 580 °C, and occasionally show a bump in the heating curve between 200 and 300 °C. The elevated Curie temperature may be a function of surface oxidation of the magnetite, while the 200–300 °C feature may be due to the Fe–Cu sulfides. Ferrar Group thermomagnetic curves are nearly reversible (Fig. 11). This set of rock magnetic parameters can be explained by the abundant homogeneous Fe–oxides observed under the SEM (Fig. 9). Rock magnetic studies on the Cape Roberts drill cores also indicate that magnetite sourced from the Ferrar Group is slightly coarser than that derived from the MVG (Sagnotti et al., 1998; Roberts

et al., 2013). In addition, Ferrar Group Fe-oxides are richer in Mn and lack Cr, another means of distinguishing between MVG and Ferrar Group Fe-oxides.

GHIC bedrock samples contain 50–400 μm homogeneous ilmenite and homogeneous magnetite. X-ray microanalysis indicates that GHIC Fe-oxides have very little cation substitution for Fe, which is responsible for their high Curie temperatures near 580 °C. Nearly pure and homogeneous magnetite, multi-domain hysteresis loops, and magnetite Curie temperatures are markers of the GHIC.

Fe-oxides grains were extremely rare in our Beacon Supergroup and Basement samples, with the exception of early Paleozoic basalts. Beacon Supergroup and Basement lithologies are weakly magnetic and their rock magnetic signatures will be masked in a sediment assemblage that also contains material derived from the MVG and Ferrar Group. However, there are some noteworthy magnetic and geochemical observations for the Beacon Supergroup and Basement lithologies. A unique

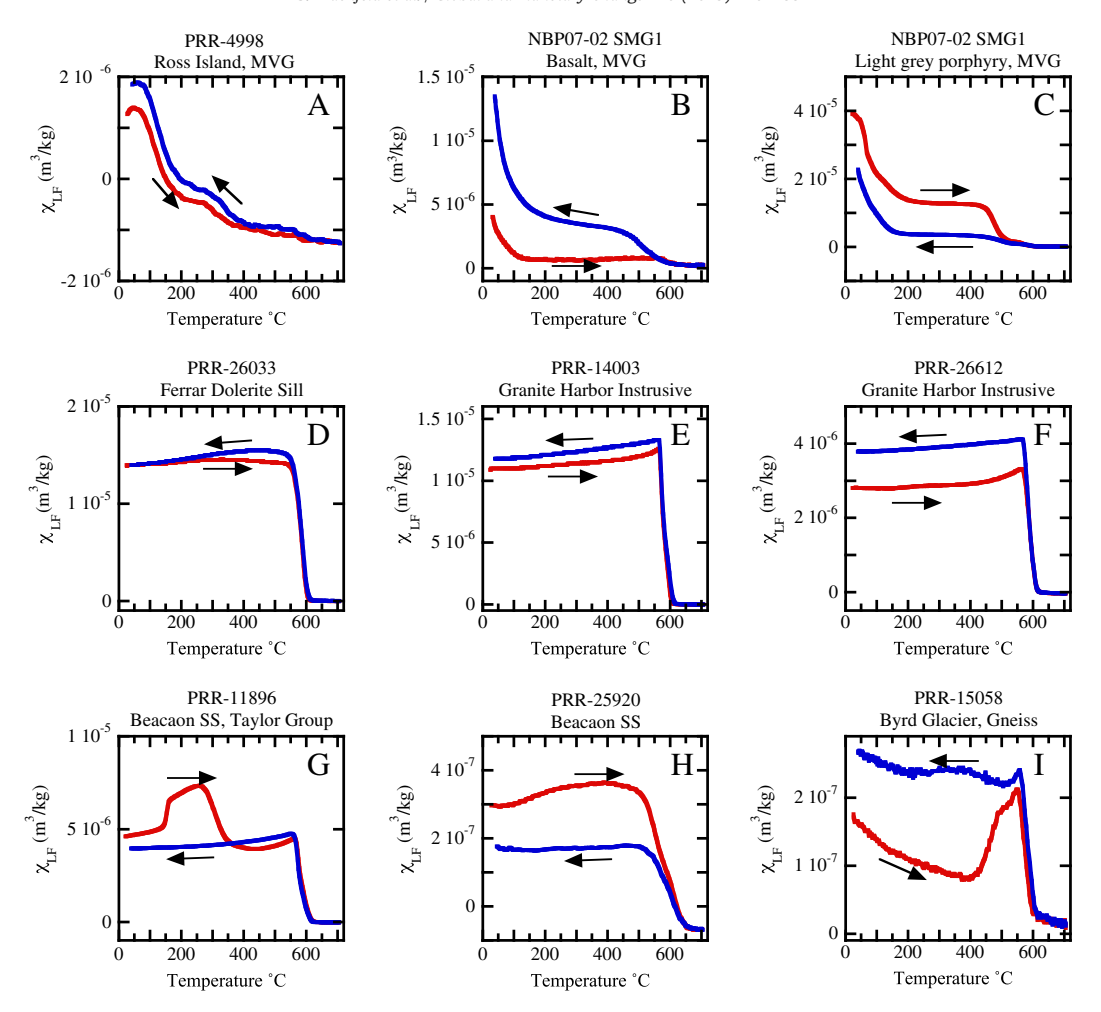


Fig. 11. Thermomagnetic curves for MVG and TAM bedrock samples. (A) PRR-4998 from Ross Island, (B) black crystalline basalt from NBP07-02 SMG1, (C) very fine grained, light gray volcanic from NBP07-02 SMG1, (D) PRR-26033 from a Ferrar Group dolerite, (E) PRR-14003 from the GHIC, (F) PRR-26612 from the GHIC, (G) PRR-18896 from the Beacon Supergroup, (H) PRR-25920 from the Beacon Supergroup, and (I) PRR-15058 from a gneiss collected near Byrd Glacier.

characteristic of Beacon Sandstone and Koettlitz gneisses is low S-ratios, in some samples below 0.8. Where observed, Beacon Sandstone Feoxides were >20 μm and had homogenous textures. The Basement samples contain the titanium minerals ilmenite, titanite, and rutile, all of which contain Mn and Nb. Gneisses from the Byrd Glacier region contain 10–20 μm pyrite grains with magnetite intergrowths along cracks and grain margins. The trace element composition of the titanium minerals coupled with detrital pyrite and multidomain hysteresis parameters are markers of the Basement metamorphics.

These bedrock characteristics allow us to explain the differences in diamictite Fe-oxide assemblages in the AND-1B core. Magnetic grain size parameters M_R/M_S, H_{CR}, and S-ratio indicate finer grains and a greater abundance of high-coercivity minerals in the upper 590 m. Thermomagnetic curves from this interval contain the 100–200 °C feature. SEM and x-ray microanalysis results from the upper 590 m indicate the presence of homogeneous titanomagnemite, Al-, Cr-, and Mg-bearing titanomagnetite, magnetite on plagioclase textures, and titanomagnetite host grains with 1–3 swarms of ilmenite lamellae. These observations are all indicative of terrigenous sediment derived from the MVG, consistent with slightly lower Fe/Ti ratios in the upper 590 m (Fig. 4; Monien et al., 2012), and clast assemblages dominated by MVG lithic fragments (Talarico et al., 2012).

AND-1B diamictites between 760 and 1285 m display multi-domain hysteresis parameters, S-ratios near to 1, Curie temperatures near 580 °C, and large homogeneous Fe-oxides. Basement, Beacon Supergroup, and GHIC lithologies control the M_R/M_S , H_{CR} , and S-ratio values

in the interval 760–1285 m. MVG-derived sediment is still present, as we continue to observe Cr-bearing titanomagnetite and 10–20 µm titanomagnetite with one set of widely-spaced ilmenite lamellae, but not the grains with three swarms of closely-spaced narrow lamellae or grains with hercynite lamellae. While the higher proportion of TAM lithologies points to a greater amount of ice sourced from TAM outlet glaciers flowing over the AND-1B drill site, it may also be due in part to fewer MVG volcanic centers within range of the ice sheet during the Miocene. The absence of the 50–200 µm titanomagnetite grains with 3 ilmenite lamellae swarms, absence of grains with hercynite lamellae, and the absence of the 100–200 °C thermomagnetic feature may indicate that these particular volcanic sources had not yet been emplaced or reached a significant size.

The combination of SEM observations, x-ray microanalysis and rock magnetic analyses allows us to match rock magnetic parameters to specific Fe-oxide populations in bedrock, thereby establishing a magnetic and microscopy signature for major bedrock units in the Ross Sea. These signatures can be applied to reconstructing past ice flow paths and ocean current flow directions, both at the AND-1B site and at more distal sites in the Ross Sea. For example, MVG derived sediment at the AND-1B site requires sediment transport from south to north, with ice entraining material eroded from volcanic centers such as Black Island, White Island, Mount Discovery, Mount Morning, and Minna Bluff en route to the AND-1B drill site. At a distal location, the presence of MVG-derived IRD would indicate a calving line northward of the MVG volcanic centers, and icebergs originating in the southwest

corner of the Ross Sea. Rock magnetic and electron microscopy signatures associated with the Ferrar Group were rare to absent in the AND-1B core. This suggests a very small contribution of sediment supplied by the Ferrar Glacier in the McMurdo Sound region and/or an ice sheet too thin to erode the higher elevation Ferrar dolerite sills.

The results presented here focus on the AND-1B diamictites, which represent glacial maxima. This strategy was selected to avoid complications from sediment reworking and redistribution by ocean currents, and to guarantee a high yield of Fe-oxides for electron microscopy. However, magnetic provenance tracers can also be applied to units representing glacial minima or transition zones. For example, we note that diatomites commonly have the highest values of H_{CR} and the lowest S-ratios within the AND-1B core. These observations could be caused by small amounts of volcanic silt and sand from nearby Ross Island, serving as indicators of icebergs, meltwater, or possibly wind-blown sediment derived from the McMurdo Sound region.

High H_{CR} and low S ratio horizons in clastic units below 760 m could be due to sediment derived from the Beacon Supergroup and/or gneisses from the Koettlitz Glacier region. If Beacon Supergroup and Koettlitz gneisses are responsible for this signature, then this requires that the edge of the Ross Ice Shelf retreated southward past the termini of the Mulock and Darwin glaciers such that calving icebergs would contain Beacon Supergroup sediment. However, the input of relatively high-coercivity magnetic minerals from Beacon Supergroup and Basement rocks may have been constant throughout the AND-1B sequence, but their rock magnetic signatures are only visible when the contribution of strongly magnetic grains from the MVG and Ferrar Group is drastically reduced.

9. Conclusions

The AND-1B drill core recovered a 13.57 Ma record of paleoclimate change within the Ross Sea region of Antarctica. The down core magnetic mineral assemblage reflects the contributions of paleoproductivity, changing sediment sources, the emergence of volcanic centers, and post-depositional diagenesis. The abundance of biogenic silica is a major control on the AND-1B rock magnetic parameters. The Miocene diamictites between 760 and 1285 m in the AND-1B core are barren of diatoms and have high values of χ_{LF} , χ_{HF} , M_R , and M_S . The Pliocene–Pleistocene interval in the upper 590 m of the AND-1B core consists of alternating diamictites, thin mudstones, and thick diatomites, interpreted as obliquity controlled glacial-interglacial cycles (Naish et al., 2009). The biogenic silica content approaches 10% in the Pliocene diamictites (McKay et al., 2009), indicating proximity to open water during their emplacement. The presence of biogenic silica dilutes the terrigenous sediment in these units and results in lower values of χ_{IF} , χ_{HF} , M_R and M_S . These differences are likely enhanced by diagenesis within the upper section of the core where organic carbon in diatomites drives dissolution of fine-grained magnetic minerals, with the exception of those protected inside lithic clasts.

Upper core and lower core diamictites also display differences in M_R/M_S, H_{CR}, S ratios, Fe-oxide grain sizes, textures, and compositions. These differences are a function of changes in sediment provenance. Here we have demonstrated that the five major bedrock groups that supply sediment to the western Ross Sea have distinctive Fe-oxide magnetic, morphologic, and compositional signatures that are transferred to the sediment derived from these rocks. MVG bedrock signatures include PSD to SSD hysteresis loops, a distinctive 100-200 °C feature in thermomagnetic curves, homogenous titanomagnemite grains with substantial Al, Mg, and Cr contents, and partially maghemitized titanomagnetite grains with 1 to 3 swarms of narrow and closely spaced ilmenite lamellae. Another distinctive texture observed in MVG samples consists of submicron magnetite outlining plagioclase laths. All of these features are observed in AND-1B diamictites between 0 and 590 m, and compositional matches can be made between Fe-Ti-Al-Mg-Cr spinels in the bedrock and sediment.

Ferrar Group Fe-oxides are micron-sized up to $50\,\mu m$ in diameter (with rare grains up to $300\,\mu m$) and have homogeneous textures. Although there is much less cation substitution in Ferrar Group Fe-oxides than in MVG Fe-oxides, Ferrar Group Fe-oxides contain more Mn and lack Cr. Ferrar Group samples are characterized by PSD to SSD hysteresis parameters and Curie temperatures very close to but slightly higher than $580\,^{\circ}$ C, possibly due to surface oxidation. Ferrar Group bedrock samples also contain Fe–Cu sulfides, which may be responsible for the $200-300\,^{\circ}$ C feature in the thermomagnetic curves. Ferrar Group signatures were rare to absent in AND-1B diamictite samples.

GHIC bedrock samples contain 50–400 µm homogeneous ilmenite and homogeneous magnetite with very little cation substitution, resulting in high Curie temperatures near 580 °C. Beacon Supergroup and Basement samples are weakly magnetic with a low abundance of Fe-oxides. However, these lithologies display low S ratios and some Beacon Supergroup samples contain maghemite. These rock magnetic signatures will be masked in a sediment assemblage that also contains material derived from the strongly magnetic MVG and Ferrar Group. The most distinctive features of the Basement lithologies are their titanium mineral assemblages. The Basement samples contain ilmenite, titanite, and rutile, all of which contain Mn and Nb. Gneisses from the Byrd Glacier region also contain 10–20 µm pyrite grains with magnetite intergrowths along cracks and grain margins.

AND-1B diamictites between 760 and 1285 m contain coarse multidomain magnetite with homogenous textures and coarse Mn-bearing ilmenite. S-ratios are near to 1 and Curie temperatures are near 580 °C. Basement, Beacon Supergroup, and GHIC lithologies control the Feoxide assemblage in diamictites between 760 and 1285 m, indicating a greater amount of ice sourced from TAM outlet glaciers. MVG-derived sediment is still present, as evidenced by Cr-bearing titanomagnetite and 10-20 µm titanomagnetite grains with one set of broad ilmenite lamellae. The 100–200 °C thermomagnetic feature is absent in diamictites from 760 to 1285 m, as are the titanomagnetites with 3 ilmenite lamellae swarms and hercynite lamellae. The volcanic centers responsible for these features may not yet have been emplaced or reached a significant size. By combining rock magnetism and electron microscopy we can match rock magnetic parameters to Fe-oxide populations within major bedrock units of the western Ross Sea, and enhance the ability to construct, interpret, and apply provenance tracers to the study of ice sheet extent and dynamics, IRD sources and dispersal patterns, and emergence of volcanic centers in the Ross Sea sector of Antarctica.

Supplementary data to this article can be found online at http://dx. doi.org/10.1016/j.gloplacha.2013.09.015.

Acknowledgments

We thank the ANDRILL MIS Science Team, drillers, curators, Raytheon Polar Services staff, and the ANDRILL Science Management Office for their efforts and assistance during the ANDRILL Program. This work was supported by a grant from the U.S. National Science Foundation via subcontract from the ANDRILL Management Office. We thank Luisa Bouhot for laboratory assistance, U.S. Polar Rock Repository curator Anne Grunow for providing guidance and samples, and Stan Jacobs for access to sediment samples from NBP07-02. The ANDRILL Program is a multinational collaboration between the Antarctic Programs of Germany, Italy, New Zealand, and the United States. Antarctica New Zealand is the project operator, and has developed the drilling system in collaboration with Alex Pyne at Victoria University of Wellington and Webster Drilling and Enterprises Ltd. Scientific studies are jointly supported by the U.S. National Science Foundation, NZ Foundation for Research Science and Technology, Royal Society of New Zealand Marsden Fund, the Italian Antarctic Research Programme (PNRA), the German Research Foundation (DFG, Project KU 683/8), and the Alfred-Wegener-Institut Helmholtz-Zentrum für Polar- und Meeresforschung, Antarctica New Zealand supported the drilling team at Scott Base; Raytheon Polar Services supported the science team at McMurdo Station and the Crary

Science and Engineering Laboratory. The ANDRILL Science Management Office at the University of Nebraska-Lincoln provided science planning and operational support. This manuscript was improved by the thoughtful comments provided by two anonymous reviewers and the GPC editorial staff.

References

- Airoldi, G., Muirhead, J.D., Zanella, E., White, J.D.L., 2012. Emplacement process of Ferrar Dolerite sheets at Allan Hills (South Victoria Land, Antarctica) inferred from magnetic fabric. Geophys. I. Int. 188. 1046–1060.
- Barrett, P., 1991. The Devonian to Triassic Beacon Supergroup of the Transantarctic Mountains and correlatives in other parts of Antarctica. In: Tingey, R.J. (Ed.), The Geology of Antarctica: Oxford Monographs on Geology and Geophysics, 17. Clarendon Press, Oxford, pp. 120–152.
- Berner, R.A., 1984. Sedimentary pyrite formation: an update. Geochim. Cosmochim. Acta 48. 605–615.
- Darby, D.A., Bischof, J.F., 1996. A statistical approach to source determination of lithic and Fe-oxide grains: an example from the Alpha Ridge, Arctic Ocean. J. Sediment. Res. 66, 599–607.
- Day, R., Fuller, M., Schmidt, V.A., 1977. Hysteresis properties of titanomagnetites: grain size and composition dependence. Phys. Earth Planet. Inter. 13, 260–267.
- Di Roberto, A., Pompilo, M., Wilsch, T., 2010. Late Miocene submarine volcanism in ANDRILL AND-1B drill core, Ross Embayment. Antarct. Geosphere 6, 524–536.
- Dunlop, D., 2002a. Theory and application of the Day plot (Mrs/Ms versus Hcr/Hc) 1. Theoretical curves and tests using titanomagnetite data. J. Geophys. Res. 107 (B3), 1–22. Dunlop, D., 2002b. Theory and application of the Day Plot (Mrs/Ms versus Hcr/Hc) 2.
- Application to data for rocks, sediments, and soils. J. Geophys. Res. 107 (B3), 1–15. Dunlop, D.J., Özdemir, Ö., 1997. Rock Magnetism: Fundamentals and Frontiers. Cambridge
- Dunlop, D.J., Ozdemir, O., 1997. Rock Magnetism: Fundamentals and Frontiers. Cambridge University Press.
- Elliot, D.H., Fleming, T.H., 2000. Weddell triple junction: the principal focus of Ferrar and Karoo magmatism during initial breakup of Gondwana. Geology 28, 539–542.
- Encarnación, J., Fleming, T.H., Elliot, D.H., Eales, H.V., 1996. Synchronous emplacement of Ferrar and Karoo dolerites and the early breakup of Gondwana. Geology 24, 535–538.
- Fielding, C.R., Browne, G.H., Field, B., Florindo, F., Harwood, D.M., Krissek, L.A., Levy, R., Panter, K.S., Passchier, S., Pekar, S.F., 2011. Stratigraphic cyclicity from the ANDRILL AND-2A drillcore, Antarctica: a long-term, ice-proximal record of Early to mid-Miocene climate, sea-level and glacial dynamism. Palaeogeogr. Palaeoclimatol. Palaeoecol. 305, 337–351.
- Findlay, R.H., Skinner, D.N.B., Craw, D., 1984. Lithostratigraphy and structure of the Koettlitz Group, McMurdo Sound, Antarctica. N. Z. J. Geol. Geophys. 27, 513–536.
- Florindo, F., Zhu, R.X., Guo, B., Yue, L.P., Pan, Y.X., Speranza, F., 1999. Magnetic proxy climate results from the Duanjiapo loess section, southernmost extremity of the Chinese loess plateau. J. Geophys. Res. 104, 645–659.
- Gunn, B.M., Warren, G., 1962. Geology of Victoria Land between the Mawson and Mulock Glaciers, Antarctica. N. Z. Geol. Surv. Bull. 71, 1–157.
- Haggerty, S.E., 1991. Oxide textures, a mini Atlas. In: Lindsley, D.H. (Ed.), Oxide Minerals: Petrologic and Magnetic Significance. Reviews of Mineralogy, 25, pp. 129–219.
- Heimann, A., Fleming, T.H., Elliot, D.H., Foland, K.A., 1994. A short interval of Jurassic continental flood basalt volcanism in Antarctica as demonstrated by ⁴⁰Ar/³⁹Ar geochronology. Earth Planet. Sci. Lett. 121. 19–41.
- Jansen, J.H.F., Van der Gaast, S.J., Koster, B., Vaars, A.J., 1998. CORTEX, a shipboard XRF scanner for element analyses in split sediment cores. Mar. Geol. 151, 143–153.
- Konfirst, M.A., Kuhn, G., Monien, D., Scherer, R.P., 2011. Correlation of Early Pliocene diatomite to low amplitude Milankovitch cycles in the ANDRILL AND-1B drill core. Mar. Micropaleontol. 80, 114–124.
- Krissek, L., Browne, G., Carter, L., Cowan, E., Dunbar, G., McKay, R., Naish, T., Powell, R., Reed, J., Wilch, T., the ANDRILL-MIS Science Team, 2007. Sedimentology and stratigraphy of the AND-1B core, ANDRILL McMurdo Ice Shelf Project, Antarctica. In: Naish, T., Powell, R., Levy, R. (Eds.), Studies from the ANDRILL, McMurdo Ice Shelf Project, Antarctica—Initial Science Report on AND-1B. Terra Antarctica, 14, pp. 185–222.
- Kyle, P.R., 1990a. McMurdo Volcanic Group, Western Ross Embayment. Introduction. In: LeMasurier, W.E., Thompson, J.W. (Eds.), Volcanoes of the Antarctic Plate and Southern Oceans: Antarctic Research Series, vol. 48. American Geophysical Union, Washington, D.C., pp. 19–25.

- Kyle, P.R., 1990b. A.III. Erebus Volcanic Province. In: Le Masurier, W.E., Thomson, J.W. (Eds.), Volcanoes of the Antarctica Plate and Southern Oceans, vol. 48. American Geophysical Union. Washington D.C., pp. 81–88.
- Kyle, P.R., Moore, J.A., Thirlwall, M.F., 1992. Petrologic evolution of anorthoclase phonolite lavas at Mount Erebus, Ross Island, Antarctica. J. Petrol. 33, 849–875.
- Licht, K.J., Lederer, J.R., Swope, R.J., 2005. Provenance of LGM glacial till (sand fraction) across the Ross Embayment, Antarctica. Quat. Sci. Rev. 24, 1499–1520.
- Liu, Q., Deng, C., Yu, Y., Torrent, J., Jackson, M.L., Banerjee, S.K., Zhu, R., 2005. Temperature dependence of magnetic susceptibility in an argon environment: implications for pedogenesis of Chinese loess/palaeosols. Geophys. J. Int. 161, 102–112.
- Martin, A., Cooper, Al, Dunlap, W., 2010. Geochronology of Mount Morning, Antarctica: two-phase evolution of a long-lived trachyte-basanite-phonolite eruptive center. Bull. Volcanol. 72, 357–371.
- McKay, R., Browne, G., Carter, L., Cowan, E., Dunbar, G., Krissek, L., Naish, T., Powell, R., Reed, J., Talarico, F., Wilch, T., 2009. The stratigraphic signature of the late Cenozoic Antarctic Ice Sheets in the Ross Embayment. Geol. Soc. Am. Bull. 121, 1537–1561.
- Monien, D., Kuhn, G., von Eynatten, H., Talarico, F.M., 2012. Geochemical provenance analysis of fine-grained sediment revealing Late Miocene to recent paleo-environmental changes in the Western Ross Sea, Antarctica. Glob. Planet. Chang. 96–97, 41–58.
- Naish, T., Powell, R., Levy, R., Wilson, G., Scherer, R., Talarico, F., Krissek, L., Niessen, F., Pompilio, M., Wilson, T., Carter, L., DeConto, R., Huybers, P., McKay, R., Pollard, D., Ross, J., Winter, D., Barrett, P., Browne, G., Cody, R., Cowan, E., Crampton, J., Dunbar, G., Dunbar, N., Florindo, F., Gebhardt, C., Graham, I., Hannah, M., Hansaraj, D., Harwood, D., Helling, D., Henrys, S., Hinnov, L., Kuhn, G., Kyle, P., Läufer, A., Maffioli, P., Magens, D., Mandernack, K., McIntosh, W., Millan, C., Morin, R., Ohneiser, C., Paulsen, T., Persico, D., Raine, I., Reed, J., Riesselman, C., Sagnotti, L., Schmitt, D., Sjunneskog, C., Strong, P., Taviani, M., Vogel, S., Wilch, T., Williams, T., 2009. Obliquity-paced Pliocene West Antarctic ice sheet oscillations. Nature 458, 322–328.
- Peters, C., Thompson, R., 1998. Magnetic identification of selected natural iron oxides and sulfides. J. Magn. Magn. Mater. 183, 365–374.
- Pompilio, M., Dunbar, N., Gebhardt, A.C., Helling, D., Kuhn, G., Kyle, P., McKay, R., Talarico, F., Tulaczyk, F., Vogel, S., Wilch, T., 2007. Petrology and geochemistry on the AND-1B core, ANDRILL McMurdo Ice Shelf Project, Antarctica. Terra Antarct. 14, 255–288.
- Ramdohr, P., 1969. The Ore Minerals and their Intergrowths. Pergammon Press (1174 pp.).
- Readman, P.W., O'Reilly, W., 1972. Magnetic properties of oxidized (cation-deficient) titanomagnetites, (Fe, Ti, [])O₄. J. Geomagn. Geoelectr. 24, 69–90.
- Roberts, A.P., Sagnotti, L., Florindo, F., Bohaty, S.M., Verosub, K.L., Wilson, G.S., Zachos, J.C., 2013. Environmental magnetic record of paleoclimate, unroofing of the Transantarctic Mountains and volcanism in Late Eocene to Early Miocene Glacimarine sediments from the Victoria Land Basin, Ross Sea, Antarctica. J. Geophys. Res. 118, 1–17
- Ross, J.I., McIntosh, W.C., Dunbar, N.W., 2012. Development of a precise and accurate agedepth model based on ⁴⁰Ar/³⁹Ar dating of volcanic material in the ANDRILL (1B) drill core, Southern McMurdo Sound, Antarctica. Glob. Planet. Chang. 96-97, 118–130.
- Sagnotti, L., Florindo, F., Wilson, G.S., Roberts, A.P., Verosub, K.L., 1998. Environmental magnetism of lower Miocene strata from the CRP-1 core, McMurdo Sound, Antarctica. Terra Antarct. 5, 661–667.
- Talarico, F.M., Sandroni, S., 2009. Provenance Signatures of the Antarctic Ice Sheets in the Ross Embayment during the Late Miocene and Early Pliocene: the ANDRILL AND-1B core record. Glob. Planet. Chang. 69, 103–123.
- Talarico, F.M., McKay, R.M., Powell, R.D., Sandroni, S., Naish, T., 2012. Late Cenozoic oscillations of Antarctic ice sheets revealed by provenance of basement clasts and grain detrital modes in ANDRILL core AND-1B. Glob. Planet. Chang. 96–97, 23–40.
- Wilson, G., Levy, R., Naish, T., Powell, R., Florindo, F., Ohneiser, C., Sagnotti, L., Winter, D., Cody, R., Henrys, S., Ross, J., Krissek, L., Niessen, F., Pompillio, M., Scherer, R., Alloway, B., Barrett, P., Brachfeld, S., Browne, G., Carter, L., Cowan, E., Crampton, J., DeConto, R., Dunbar, G., Dunbar, R., von Eynatten, H., Gebhardt, C., Giorgetti, S., Graham, I., Hannah, M., Hansaraj, D., Harwood, D., Hinnov, L., Jarrard, R., Joseph, L., Kominz, M., Kuhn, G., Kyle, P., Laufer, A., McIntosh, W., McKay, R., Maffioli, P., Magens, D., Millan, C., Monien, D., Morin, P., Paulsen, T., Pollard, D., Raine, J., Riesselman, C., Sandroni, S., Schmitt, D., Sjunneskog, C., Strong, P., Talarico, F., Taviani, M., Villa, G., Vogel, S., Wilch, T., Williams, T., Wilson, T., Wise, S., 2012. Neogene tectonic and climatic evolution of the western Ross Sea, Antarctica—chronology of events from the AND-1B drillhole. Glob. Planet. Chang. 96–97, 189–203.
- Winter, D., Sjunneskog, C., Scherer, R., Maffioli, P., Harwood, D.M., 2012. Diatom-based correlation of early to mid-Pliocene drillcores from the southwestern Ross Sea, Antarctica. Glob. Planet. Chang. 96–97, 131–142.